Author/s:
Wang, J;Gleeson, PA;Fourriere, L

Title:
Spatial–Temporal Mapping Reveals the Golgi as the Major Processing Site for the Pathogenic Swedish APP Mutation: Familial APP Mutant Shifts the Major APP Processing Site

Date:
2024-03-01

Citation:
Wang, J., Gleeson, P. A. & Fourriere, L. (2024). Spatial–Temporal Mapping Reveals the Golgi as the Major Processing Site for the Pathogenic Swedish APP Mutation: Familial APP Mutant Shifts the Major APP Processing Site. Traffic, 25 (3), https://doi.org/10.1111/tra.12932.

Persistent Link:
https://hdl.handle.net/11343/345465

Traffic

WILEY

Traffic

RESEARCH ARTICLE OPEN ACCESS

Spatial–Temporal Mapping Reveals the Golgi as the Major Processing Site for the Pathogenic Swedish APP Mutation: Familial APP Mutant Shifts the Major APP Processing Site

Jingqi Wang | Paul A. Gleeson | Lou Fourriere

The Department of Biochemistry and Pharmacology, Bio21 Molecular Science and Biotechnology Institute, The University of Melbourne, Parkville, Victoria, Australia

Correspondence: Paul A. Gleeson (pgleeson@unimelb.edu.au) | Lou Fourriere (lou.fourriere@unimelb.edu.au)

Received: 16 October 2023 | **Revised:** 13 February 2024 | **Accepted:** 1 March 2024

Funding: This work was supported by National Health and Medical Research Council (Grant APP1163862: 2013384). J.W. is supported by a University of Melbourne International Postgraduate Award.

Keywords: amyloid beta | amyloid precursor protein (APP) | APP Icelandic mutation | APP Swedish mutation | endosomes | familial Alzheimer's disease | Golgi apparatus | live cell imaging | membrane trafficking | RUSH system

ABSTRACT

Alzheimer's disease is associated with increased levels of amyloid beta (Aβ) generated by sequential intracellular cleavage of amyloid precursor protein (APP) by membrane-bound secretases. However, the spatial and temporal APP cleavage events along the trafficking pathways are poorly defined. Here, we use the Retention Using Selective Hooks (RUSH) to compare in real time the anterograde trafficking and temporal cleavage events of wild-type APP (APPwt) with the pathogenic Swedish APP (APPswe) and the disease-protective Icelandic APP (APPice). The analyses revealed differences in the trafficking profiles and processing between APPwt and the APP familial mutations. While APPwt was predominantly processed by the β-secretase, BACE1, following Golgi transport to the early endosomes, the transit of APPswe through the Golgi was prolonged and associated with enhanced amyloidogenic APP processing and Aβ secretion. A 20°C block in cargo exit from the Golgi confirmed β- and γ-secretase processing of APPswe in the Golgi. Inhibition of the β-secretase, BACE1, restored APPswe anterograde trafficking profile to that of APPwt. APPice was transported rapidly through the Golgi to the early endosomes with low levels of Aβ production. This study has revealed different intracellular locations for the preferential cleavage of APPwt and APPswe and Aβ production, and the Golgi as the major processing site for APPswe, findings relevant to understand the molecular basis of Alzheimer's disease.

1 | Introduction

Alzheimer's disease is the most common cause of dementia, characterised by cognitive and behavioural progressive disabilities, and represents a considerable burden for our ageing society [1, 2]. Alzheimer's disease is a complex neurological disease strongly associated with the production of neurotoxic amyloid beta (Aβ) and amyloid plaques, which are hallmarks of the disease [3–5]. The significance of the amyloid production pathway in Alzheimer's disease is emphasised by familial mutations responsible for inherited, early-onset, Alzheimer's disease (EOAD). There is currently no effective cure for Alzheimer's disease, in part due to a lack of knowledge on the basic molecular and cellular mechanisms of the disease [2, 6, 7].

Abbreviations: AD, Alzheimer's disease; APP, amyloid precursor protein; APPice, Icelandic APP; APPswe, Swedish APP; APPwt, wild-type APP; Aβ, amyloid beta; BACE1, beta site APP-cleaving enzyme; EE, early endosomes; EOAD, early-onset Alzheimer's disease; ER, endoplasmic reticulum; LE, late endosomes; RE, recycling endosomes; TGN, *trans*-Golgi network; TIRF, total internal reflection fluorescence microscopy.

The last two authors contributed equally to this work.

Aβ production results from intracellular proteolytic processing of the amyloid precursor protein (APP) by different membrane-bound secretases [8–10]. In the non-amyloidogenic pathway, APP is cleaved by the α-secretase to generate the soluble ectodomain, sAPPα, and a membrane-bound fragment called C83 (also known as CTF-α). C83 is then rapidly cleaved by the γ-secretase to generate p3, a non-neurotoxic product. In contrast, in the amyloidogenic pathway, APP is cleaved by the β-secretase, BACE1, to produce the soluble APPβ ectodomain, sAPPβ, and C99 (also called CTF-β) [11–13]. C99 is further cleaved by γ-secretase, which leads to the production of Aβ peptides; Aβ is secreted from the cell, and oligomerises and aggregates into amyloid plaques [5]. Many of the familial disease-associated mutations are mapped to the coding region of APP or γ-secretase, highlighting the importance of APP processing in Alzheimer's disease [14]. Therapeutic monoclonal antibodies have been recently developed (i.e., aducanumab, lecanemab and donanemab), which bind to extracellular plaques and extracellular Aβ aggregates, but fail to inhibit the intracellular production of Aβ, which is a critical pathological feature of the disease [15].

APP cleavage by BACE1 is the rate-limiting step for Aβ production and the co-localisation of the two integral membrane proteins in the same cellular sub-compartment is required for BACE1-mediated processing (reviewed in [4, 5]). Work by our laboratory and other groups have shown that changes in the intracellular trafficking of APP and/or BACE1 directly affect the production of Aβ [16–19]. APP and BACE1 are segregated into distinct subdomains in the early Golgi and are subsequently transported from the Golgi into distinct transport pathways [16, 20–22]; although the majority of APP is trafficked directly to the early endosomes, BACE1 is transported from the *trans*-Golgi network (TGN) to the cell surface and then endocytosed by clathrin-mediated endocytosis into early endosomes [17, 23]. Hence, endosomes are usually considered the major site for the processing of wild-type APP (APPwt) by BACE1 and γ-secretase [24–26]. However, in addition to endosomes, the Golgi apparatus represents a potential site for APP and BACE1 co-localisation and APP processing [21, 27, 28]. Perturbation of the Golgi residency time of APP or BACE1 results in elevated Aβ production [16, 21, 22, 27].

Familial mutations leading to EOAD, and animal models, have shown that increased processing of APP results in increased levels of Aβ, which seeds the onset of the disease [3, 5]. Therefore, to understand the initiation of Alzheimer's disease, it is essential to define the intracellular trafficking and processing of familial APP and how it may differ from APPwt. The trafficking and processing of the Swedish familial APP mutation (APPswe) (the most well studied of the familial mutants) has been investigated in both the secretory and endocytosis pathways with a range of conclusions. The majority of studies to date indicate that APPswe is processed predominantly in the secretory pathway [10, 28–30], although some studies suggest the endocytic pathway is also involved [30–33]. Of relevance to this current study, studies in the 1990s indicated a role for the secretory pathway by the detection of β-secretase cleavage products of APPswe in APPswe-transfected cells [10, 28–30]. Nonetheless, their conclusions differed in the identity of the APP processing site along the secretory pathway. For example, processing was suggested to take place in post-Golgi vesicles, based on the detection of the soluble APPswe-β (BACE1 cleaved luminal fragment of APPswe) by immunofluorescence [29], whereas APPswe-derived Aβ was reported to be enriched in both Golgi/TGN and nascent post-TGN vesicles [10]; the latter finding suggesting that the Golgi, rather than post-Golgi vesicles, may be the major location for Aβ production from APPswe. Data from pulse-chase experiments by Thinakaran et al. [28] proposed that the BACE1 product of APPswe, CTF-β (C99), was generated in the early Golgi, although this proposal appears inconsistent with an acidic pH required for BACE1 activity. A FRET study has also confirmed an interaction between APPswe and BACE1 in the Golgi apparatus [31]. Many of the early studies were performed following drug treatment and detailed high-resolution imaging of APP was not carried out. To better define the trafficking and processing of APPswe, a quantitative analysis of the APP processing events along the secretory pathway needs to be performed in real time. Technical advances over the past 10 years now provide for the opportunity to extend these earlier studies and re-visit the identification of the major sites of APP processing of both the wild-type and familial APP mutants.

Here we have combined the Retention Using Selective Hooks (RUSH) system [34] to follow in real time the trafficking of the newly synthesised APP and to identify the temporal events of APP cleavage over time. The innovative combined analysis provides a spatial and temporal map of the trafficking and processing of APPwt. In addition, we have compared the effect of two well-known familial APP mutations on APP trafficking and processing along the secretory pathway. The Swedish APP (APPswe) is a well-established pathogenic double mutation associated with high levels of Aβ production [35, 36]. The Icelandic APP (APPice) is the only known mutation with a protective role against Alzheimer's disease and is associated with low levels of Aβ production [37]. Our study reveals that APP mutants have distinct trafficking profiles and secretase processing. The Golgi transit of newly synthesised APPswe is associated with enhanced processing by β-secretase and enhanced Aβ production, compared with APPwt, while APPice traffics rapidly through the Golgi and is associated with low levels of β-secretase cleavage and a preferential production of fragments associated with the α-secretase pathway. These results highlight the importance of the secretory pathway in the processing of APP and the Golgi apparatus in the production of intracellular Aβ. This study has also identified preferential intracellular locations for the cleavage of APPwt and APPswe.

2 | Results

2.1 | Real-Time Anterograde Trafficking Kinetics and Itinerary of APPwt

To define the intracellular trafficking itinerary and transport kinetics of APP, we synchronised the anterograde trafficking of APP from the endoplasmic reticulum (ER) in live cells using the RUSH system [34]. In the RUSH system, two fusion proteins are expressed: a 'hook' fused to the streptavidin (str-) molecule and the cargo protein of interest fused to streptavidin-binding peptide (SBP) and a fluorescence tag (i.e., mScarlet) (Figure 1A). The hook used in this study was the human invariant chain (Ii), a membrane protein with an ER retention motif [38]. The SBP and the fluorescent tag were fused at the C-terminus of full-length wild-type APP_{695}, a type I transmembrane protein. In the absence of biotin, the newly synthesised APP would be retained in the ER through the interaction between the streptavidin molecule and SBP (Figure 1A), and upon biotin addition, APP

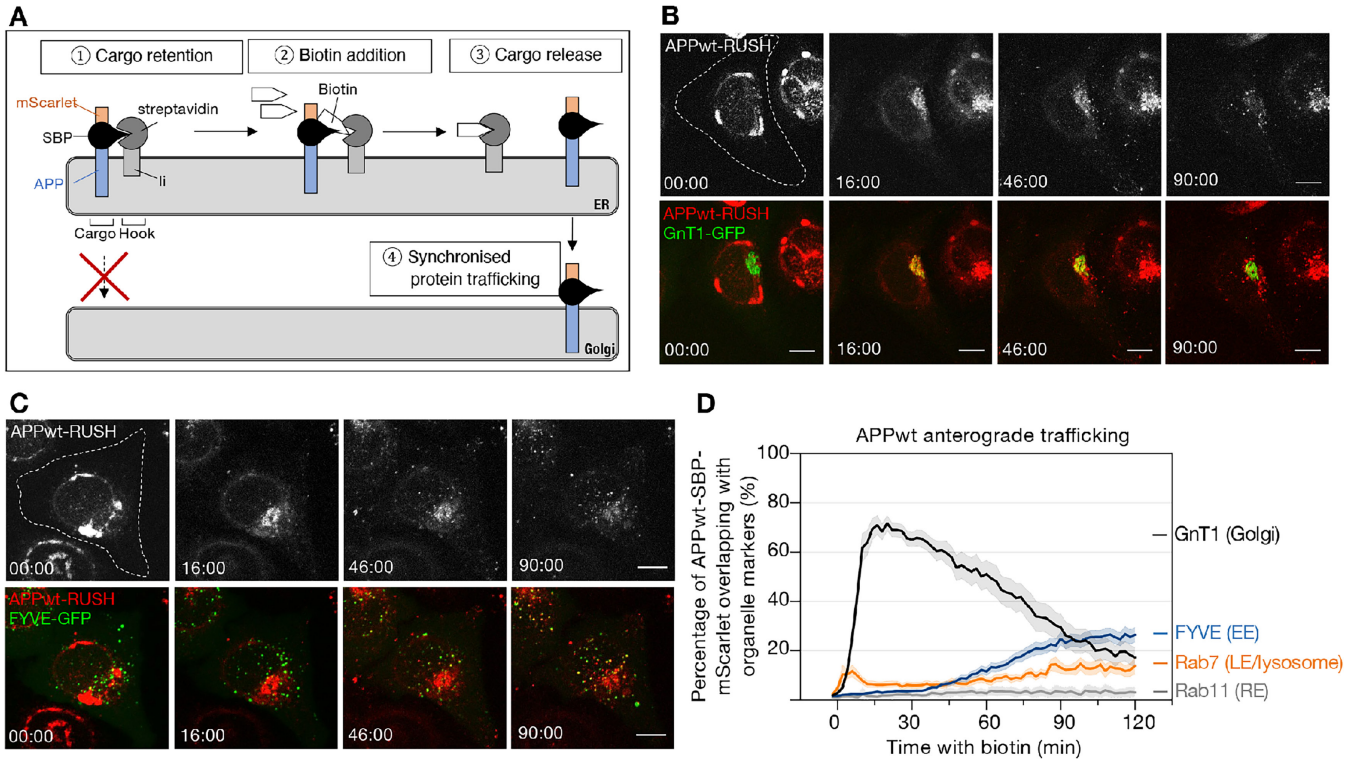

FIGURE 1 | Anterograde trafficking of APPwt. (A) Synchronisation of the anterograde trafficking of APPwt using the RUSH system. In the absence of biotin, APP is retained in the ER through the interaction between streptavidin peptide (SBP) fused to APP with a streptavidin molecule (Str) fused to a hook (Ii). APP cargoes are released in synchronisation by addition of biotin and are followed using its fluorescent tag mScarlet. (B,C) Monolayers of HeLa E2 cells stably expressing Str-Ii and APPwt-SBP-mScarlet (red) were transfected with indicated organelle marker constructs for 24 h. GnT1-GFP (B, green) and FYVE-GFP (C, green) label the Golgi apparatus and the early endosomes, respectively. Biotin was added at time 00:00 min:s, and real-time dual-colour images of live cells were acquired at the indicated time points (min:s) after biotin addition using a spinning disc microscope. Images show maximum projections of z-stacks (11 optical sections). Scale bar represents 10 μm. For other organelle markers, see Figure S1. (D) Quantification of the overlap of APPwt-SBP-mScarlet (red) with each organelle marker (GnT1 for the Golgi, FYVE for the early endosomes, Rab7 for the late endosomes, lysosomes and Rab11 for the recycling endosomes) in individual HeLa E2 cells from (B) and the percentage of co-localisation were calculated using a Mander's coefficient from z-stacks using FIJI/ImageJ [39]. Each curve represents mean value ± SEM (shown in shaded bars), $n \geq 17$ cells for each group from three independent experiments.

molecules would be released rapidly in synchronisation and the trafficking of APP from the ER can be tracked.

A HeLa cell line stably expressing Str-Ii and APPwt-SBP-mScarlet (also referred to as 'HeLa E2') was generated to provide uniform expression of APPwt-RUSH and allow quantitative analysis. To track the kinetics of APP trafficking, HeLa E2 cells were transiently transfected with the following organelle markers: GnT1-GFP (Golgi), FYVE-GFP (early endosome), Rab7-GFP (late endosome/lysosome) or Rab11-GFP (recycling endosome), and dual-colour live cell imaging was performed over a 2-h period. Biotin was added at time point 00:00 min:s to release APPwt-SBP-mScarlet from the ER (Figure 1B,C, Movies S1 and S2). The degree of co-localisation between APPwt-SBP-mScarlet and each organelle marker throughout the biotin time course was quantitated semi-automatically from three independent experiments ($n \geq 17$ cells) using an unbiased batch analysis Fiji macro [39] (Figure 1D). In the absence of biotin (0 min), the degree of co-localisation between APPwt-SBP-mScarlet with all four markers was minimal (<5%) (Figure 1B–D). By 15 min after the addition of biotin, approximately 71% of APPwt-SBP-mScarlet co-localised with the Golgi marker, GnT1-GFP (Figure 1B,D). From 30 min after biotin addition, the degree of overlap of APPwt-SBP-mScarlet with GnT1-GFP declined, while it increased with FYVE-GFP (Figure 1C,D, Movie S2). These data indicate that the newly synthesised APPwt-SBP-mScarlet traffics from the ER to the Golgi and then to the early endosomes. The degree of overlap between APPwt-SBP-mScarlet and Rab7-GFP increased from <5% to 10%, 75 min after biotin addition, indicating transport of a portion of APPwt-SBP-mScarlet to the late endosome/lysosomes for degradation (Figures 1D and S1A). There was minimal co-localisation between APPwt-SBP-mScarlet and Rab11-GFP (recycling endosomes) throughout the time course (<10%) (Figures 1D and S1B). The intracellular distribution of APPwt-SBP-mScarlet after 120 min of biotin addition (Figure 1D) is comparable with the intracellular distribution of untagged APP under steady-state conditions [22], which indicates that the APP localisation and trafficking of APPwt-SBP-mScarlet is not affected by the RUSH system.

2.2 | Spatial and Temporal Secretase Processing of APPwt Along the Secretory Pathway

APP undergoes a series of cleavage events executed by different secretases (Figure 2A). Full-length APP can be initially cleaved by either the α- or the β-secretase, generating C-terminal membrane fragments C83 or C99, respectively. Both C83 and C99 fragments are subject to further cleavage by the γ-secretase,

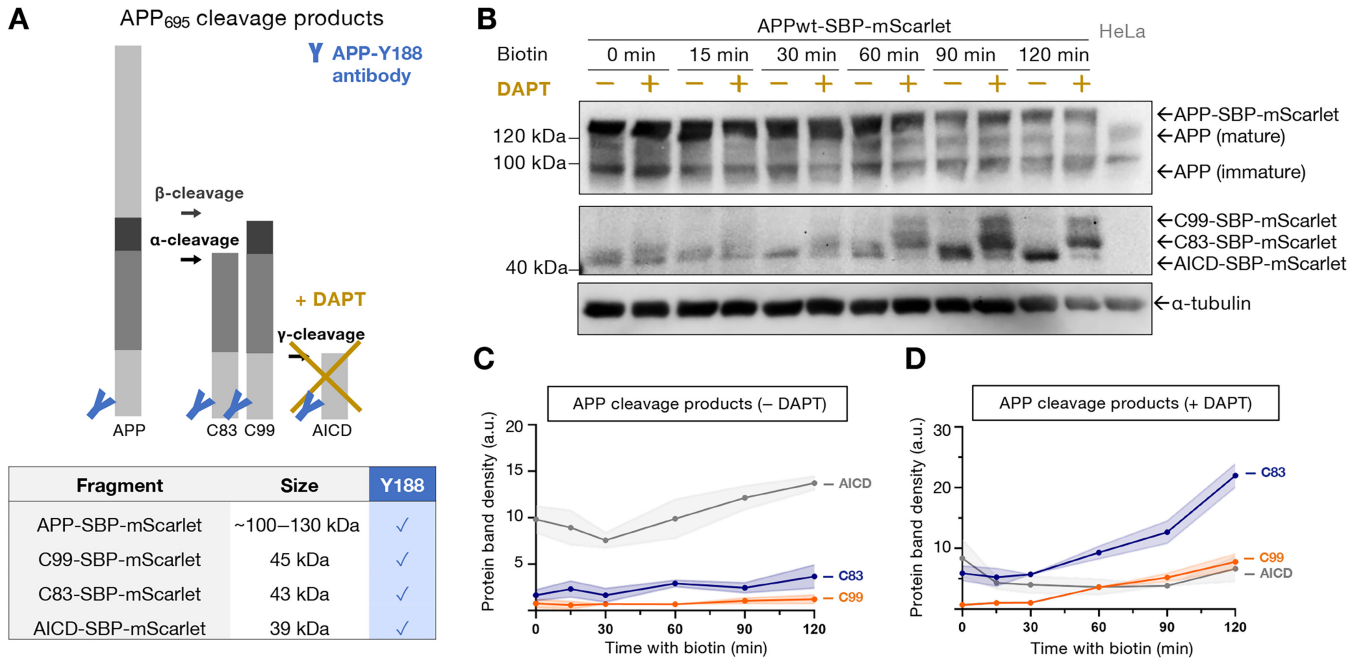

Fragment	Size	Y188
APP-SBP-mScarlet	~100–130 kDa	✓
C99-SBP-mScarlet	45 kDa	✓
C83-SBP-mScarlet	43 kDa	✓
AICD-SBP-mScarlet	39 kDa	✓

FIGURE 2 | APPwt processing along the secretory pathway. (A) Sequential cleavage of full-length APP by the α, β and γ-secretases leads to the formation of C83, C99 and AICD fragments. APP full length and APP fragments have different molecular weight and are all recognised on their C-terminus using the APP-Y188 antibody. DAPT treatment inhibits the γ-cleavage and therefore the conversion of C83 or C99 in AICD fragments. (B) Monolayers of HeLa E2 cells stably expressing Str-Ii and APPwt-SBP-mScarlet (red) were treated with either a carrier control (DMSO) or an inhibitor of the γ-secretase (DAPT, 500 nM) for 16 h. Cells were lysed at different time points after biotin addition and were analysed by immunoblotting using APP-Y188 antibody. Blot is representative of three independent experiments. (C,D) Protein levels of C83-SBP-mScarlet, C99-SBP-mScarlet and AICD-SBP-mScarlet fragments were quantified from three independent immunoblots and normalised to the total protein stained as described in Section 4 (see Figure S2A). Each curve represents mean ± SEM from three independent experiments.

giving rise to the final C-terminal membrane fragment, AICD (Figure 2A).

To explore the spatial and temporal secretase-mediated processing events of APP through the secretory pathway, we took advantage of the RUSH system and assessed the timing of the generation of cleavage products of APPwt-SBP-mScarlet at different time points after biotin addition by immunoblotting (Figure 2). APP C-terminal cleavage products can be readily separated on the basis of size using the APP-Y188 antibody, which recognises residues 682–687 close to the C-terminal of APP (Figure 2A). Hence, APP-Y188 antibody detects full-length APP, both the β- and the α-secretase products (C99 and C83, respectively), as well as the subsequent γ-secretase cleavage product, AICD (Figure 2A). APPwt-SBP-mScarlet, C99-SBP-mScarlet, C83-SBP-mScarlet and AICD-SBP-mScarlet fragments have an additional mass of 28 kDa compared with the endogenous APP, contributed by the SBP-mScarlet polypeptide. To confirm the identity of the small fragments generated, the γ-secretase inhibitor DAPT was used; in the presence of DAPT, C99 and C83 fragments were protected from γ-secretase cleavage, and AICD was not generated (Figure 2A,B).

The broad band detected in HeLa E2 cells of >120 kDa at 0 min of biotin corresponds to the size of full-length APP-SBP-mScarlet and likely represents the immature glycosylated species (Figure 2B). Endogenous full-length APP was also detected in E2 cells and untransfected HeLa cells, consisting of two bands of ~100 and 115 kDa (Figure 2B), representing immature and mature glycosylated proteins, which has been consistently reported previously [40–42]. In addition, three distinct bands were detected between 40 and 50 kDa after biotin addition in HeLa E2 cells treated with DAPT, or not. The band detected at 40 kDa without DAPT decreased in the presence of DAPT, which indicated the band was AICD-SBP-mScarlet. In contrast, the bands at 43 and 45 kDa were more intense in the presence of DAPT (Figure 2B), indicating that these proteins represent C99-SBP-mScarlet and C83-SBP-mScarlet, respectively. The time-course analysis shows that the full-length APPwt-SBP-mScarlet (~120 kDa) gradually decreased over the 2-h time course (Figure 2B). In the absence of DAPT, C83-SBP-mScarlet and C99-SBP-mScarlet were barely detectable throughout the 2-h time course (Figure 2B,C), indicating that the intermediate α- and β-cleavage products are rapidly cleaved by γ-secretase into AICD-SBP-mScarlet. In the absence of DAPT, low levels of AICD-SBP-mScarlet were detected in the ER (0 min biotin) and AICD increased gradually after APPwt release from the ER, from 30 min onwards after biotin addition (Figure 2B,C). In the presence of DAPT, the levels of both C99-SBP-mScarlet and C83-SBP-mScarlet products increased significantly from 30 min after biotin addition (Figure 2B,D). The level of the α-secretase cleavage product, C83-SBP-mScarlet, was three-fold higher than the level of the β-secretase cleavage product C99-SBP-mScarlet (Figure 2D). Hence, in HeLa cells, the majority of APPwt is processed along the non-amyloidogenic pathway and a smaller proportion is cleaved by β-secretase along the amyloidogenic pathway. Live imaging data from Figure 1 show that APPwt-SBP-mScarlet is predominately in the Golgi at 30–45 min after biotin addition and in both the Golgi and endosomes at 60–90 min after biotin addition. Taken together, these data indicate that the

secretase processing of newly synthesised APPwt may be initiated in the Golgi and then continues as APPwt is trafficked to the endosomes. Hence, the detection of APP cleavage products using the RUSH system revealed the temporal and spatial APP processing events following the exit of newly synthesised APP from the ER.

2.3 | Intracellular Distribution of APP Is Altered by the Swedish and Icelandic Mutations

Numerous familial APP mutations have been identified in Alzheimer's disease and are found either flanking or within the transmembrane domain of APP (Figure 3A). Most studies to

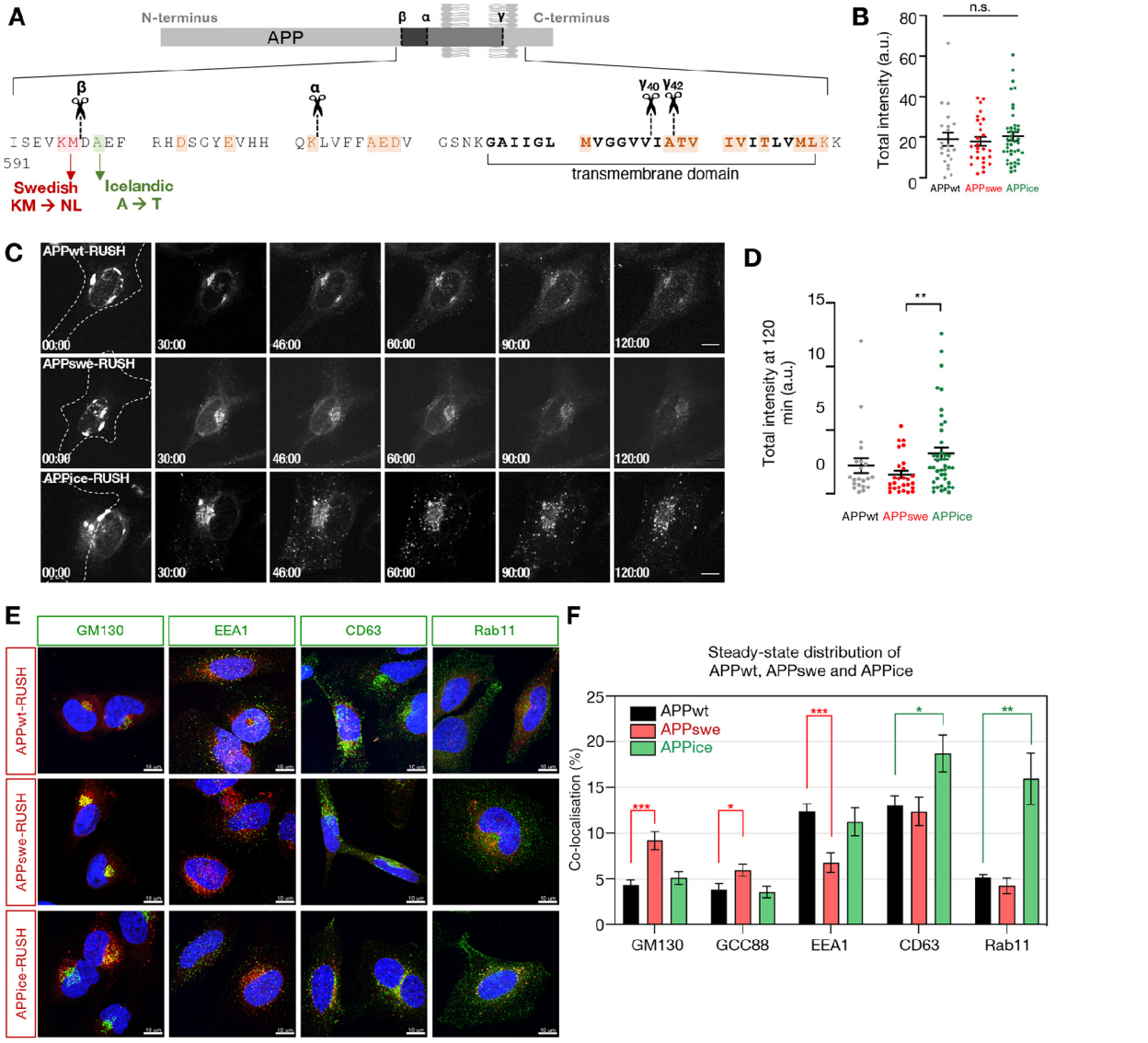

FIGURE 3 | APP cellular distribution is altered by the Swedish and Icelandic mutations. (A) Sequence of APP protein around the transmembrane domain (represented in bold). The secretases cleavage sites are highlighted by the scissors, with the Swedish and the Icelandic mutations shown in red and green, respectively; other known pathogenic APP mutations identified in familial Alzheimer's disease are labelled in orange. (B–D) Monolayers of HeLa cells stably expressing WT-, Swedish- or Icelandic-APP RUSH constructs (clone E2, C7 or F10, respectively, red) were imaged every 2 min for 2 h using a spinning disc microscope. (B) Total signal intensities in individual cells at the start (0 min) of the time-lapse imaging. Each dot represents an individual cell with mean ± SEM, $n \geq 21$ for each group from three independent experiments. n.s., not significant, analysed by two-tailed *t*-test with Welch's correction. (C) Biotin was added at time 00:00 (min:s). Images show maximum projections of z-stacks. Scale bar represents 10 μm. (D) Total signal intensities in individual cells at the end (120 min) of the time-lapse imaging. Each dot represents an individual cell with mean ± SEM, $n \geq 21$ for each group from three independent experiments. **, $p < 0.01$ analysed by two-tailed *t*-test with Welch's correction. (E) Monolayer of HeLa cells stably expressing Str-Ii and APPwt-, Str-Ii and APPswe- or Str-Ii and APPice-SBP-mScarlet (E2, C7 and F10, respectively) (red) were fixed 2 h after biotin addition (steady state), permeabilised and blocked. Cells were stained with anti-GM130, GCC88, EEA1, CD63 and Rab11 antibodies (green), to identify co-localisation between APP (red) with *cis*-Golgi, *trans*-Golgi, early endosomes, late endosome/lysosomes and recycling endosomes, respectively. Images were taken using a Zeiss LSM880 Airyscan with 63× oil objective in SR mode and z-stacks were deconvolved using Huygens software (conservative deconvolution mode). Scale bar represents 10 μm. (F) Co-localisation coefficient (intensity) analysed for APP and different organelle markers were calculated using Imaris. Data are represented as the mean ± SEM, $n \geq 13$ cells from three independent experiments. *$p < 0.05$, **$p < 0.01$ and ***$p < 0.001$ analysed by two-tailed *t*-test with Welch's correction.

date have focused on analysing the substrate affinity of mutated APP for the β- or the γ-secretases; the impact of the familial APP mutations on the intracellular APP trafficking, intracellular APP distribution and intracellular APP processing have not yet been rigorously characterised. Here, we have investigated the effect of two familial APP mutations, namely the Swedish and the Icelandic, on the intracellular transport and processing of APP. The APPswe is a well-established pathogenic APP mutation that gives rise to elevated levels of Aβ, while the APPice generates low levels of Aβ and is the only known mutation with a protective role against the disease progression [36, 37].

The Swedish and Icelandic mutations were introduced into APPwt-RUSH plasmid. Two HeLa cell lines stably expressing Str-Ii and APPswe-SBP-mScarlet (HeLa C7) and Str-Ii and APPice-SBP-mScarlet (HeLa F10) were generated. Total mScarlet intensity in the absence of biotin was similar for WT and the two APP mutant stable cell lines (Figure 3B), which indicates a similar expression level of the APP-SBP-mScarlet proteins in the three monoclonal stable cell lines. Moreover, ER retention of APP was observed in the three cell lines in the absence of biotin. To define the trafficking itinerary and transport kinetics of APPswe and APPice, live cell imaging was carried out for HeLa C7 and F10 cell lines, as for HeLa E2 cells. After biotin addition, newly synthesised APP was released from the ER, transported to the Golgi apparatus and subsequently sorted to vesicular structures dispersed throughout the cytosol (Figure 3C). Therefore, both APPswe- and APPice-SBP-mScarlet displayed a similar trafficking path as APPwt-SBP-mScarlet. However, differences were observed in the trafficking kinetics and signal lifetime of the two APP mutants; from 60 min after biotin, while APPswe-SBP-mScarlet signal became very dim with very few fluorescent puncta, APPice-SBP-mScarlet was associated with abundant and bright puncta (Figure 3C). The average total intensity in the cells expressing APPice-SBP-mScarlet was higher than that in cells expressing APPswe-SBP-mScarlet 120 min after biotin addition (end of the time course similar to the steady-state) (Figure 3D). The localisation of the APP proteins was quantified at 120 min using organelle markers. APPswe-SBP-mScarlet was enriched in the Golgi compared with APPwt-SBP-mScarlet (Figure 3E,F). In contrast, APPice-SBP-mScarlet was enriched in late endosomes and recycling endosomes compared with APPwt-SBP-mScarlet (Figure 3E,F). Hence, Swedish and APPice mutations displayed distinct intracellular distributions at steady state, which also differed from APPwt. These differences in intracellular distribution may be explained by changes in their trafficking kinetics and/or variation in their intracellular processing, leading to a differential cleavage rate.

2.4 | Swedish and APPice Mutants Differ in Trafficking Kinetics Through the Golgi and to the Early Endosomes

The Golgi apparatus, in addition to the early/late endosomes, represents a site for β-secretase cleavage of APP [5]. As APPswe and APPice showed differences in the level of the APP protein in the Golgi and endosomes at steady state, the kinetics of APPswe and APPice transport through the Golgi was compared with that of APPwt, using GnT1-GFP to highlight the Golgi (Figure 4A,B, Movies S3–S5). APPswe-SBP-mScarlet, APPice-SBP-mScarlet and APPwt-SBP-mScarlet reached the Golgi 15 min after biotin addition; however, the percentage of total APPswe fluorescence overlapping with GnT1-GFP was lower (42%) compared with those of APPwt or APPice (~70%) (Figure 4A,B). Furthermore, the rate of Golgi exit of APPswe was considerably slower compared with those of APPwt and APPice. Notably, the total intensity of the APPswe-SBP-mScarlet signal was routinely observed to decline rapidly during its transit through the Golgi (Figure 4A, Movie S4). The turnover of APPwt-SBP-mScarlet and APP RUSH mutants was assessed after biotin addition in the presence of cycloheximide to inhibit the synthesis of new APP proteins during the pulse with biotin (Figure S3A). APPswe-SBP-mScarlet fluorescence waned more rapidly than APPwt and APPice (Figure S3B), and full-length APPswe-SBP-mScarlet detected by immunoblotting was more rapidly turned over than APPwt and APPice (Figure S3C,D), confirming that the loss of APPswe-SBP-mScarlet after biotin addition was due to a rapid processing and/or degradation of APPswe following biotin addition. Also of note, the Golgi apparatus was found to be dispersed in some HeLa cells expressing APPswe-SBP-mScarlet, as monitored with the Golgi marker GnTI-GFP (e.g., see Movie S4).

APPwt and APPice had a similar half-life after addition of biotin (Figure S3), but in contrast to APPwt-SBP-mScarlet, APPice-SBP-mScarlet was observed to exit the Golgi at a faster rate than APPwt (Figure 4A,B, Movies S3 and S5). By 60 min after biotin addition, the majority of APPice-SBP-mScarlet had exited the Golgi with only 21% of the APPice pool co-localised with GnT1-GFP, whereas there was 51% of APPwt within the Golgi (Figure 4B). This analysis directly demonstrates that the disease-protective APPice traffics through the Golgi with a faster rate than APPwt or APPswe, whereas the trafficking of the pathogenic APPswe is retarded.

As early endosomes are one of the major sites for APP processing, we quantified the kinetics of co-localisation of APPwt, APPswe and APPice with the early endosome marker FYVE-GFP in live cells (Figure 4C,D). APPice and APPwt cargoes started to overlap with FYVE-GFP at 35 and 60 min after biotin addition, respectively, which corresponds to their respective Golgi exit times (Figure 4C,D). However, the intensity of APPswe-SBP-mScarlet overlapping with the FYVE-positive compartments was considerably lower with very little increase during the time course, indicating a low arrival of APPswe-SBP-mScarlet cargo to the early endosomes (Figure 4C,D). Interestingly, there was a 2.5-fold higher level of APPice-SBP-mScarlet at the early endosomes from 60 min of biotin addition compared with APPwt-SBP-mScarlet, indicating APPice-SBP-mScarlet was delivered to early endosomes more efficiently than APPwt (Figure 4C,D), consistent with a faster transport rate of APPice-SBP-mScarlet through the Golgi (Figure 4A,B). Therefore, the APP Swedish and Icelandic mutations have different trafficking kinetics through the Golgi and to the early endosomes, which is consistent with their different distribution at steady state (Figure 3E).

2.5 | Delivery of APP to the Cell Surface Is Minimal but Altered by the Swedish or Icelandic Mutation

Previous work from our laboratory demonstrated that the majority of APP is transported directly from the TGN to the early

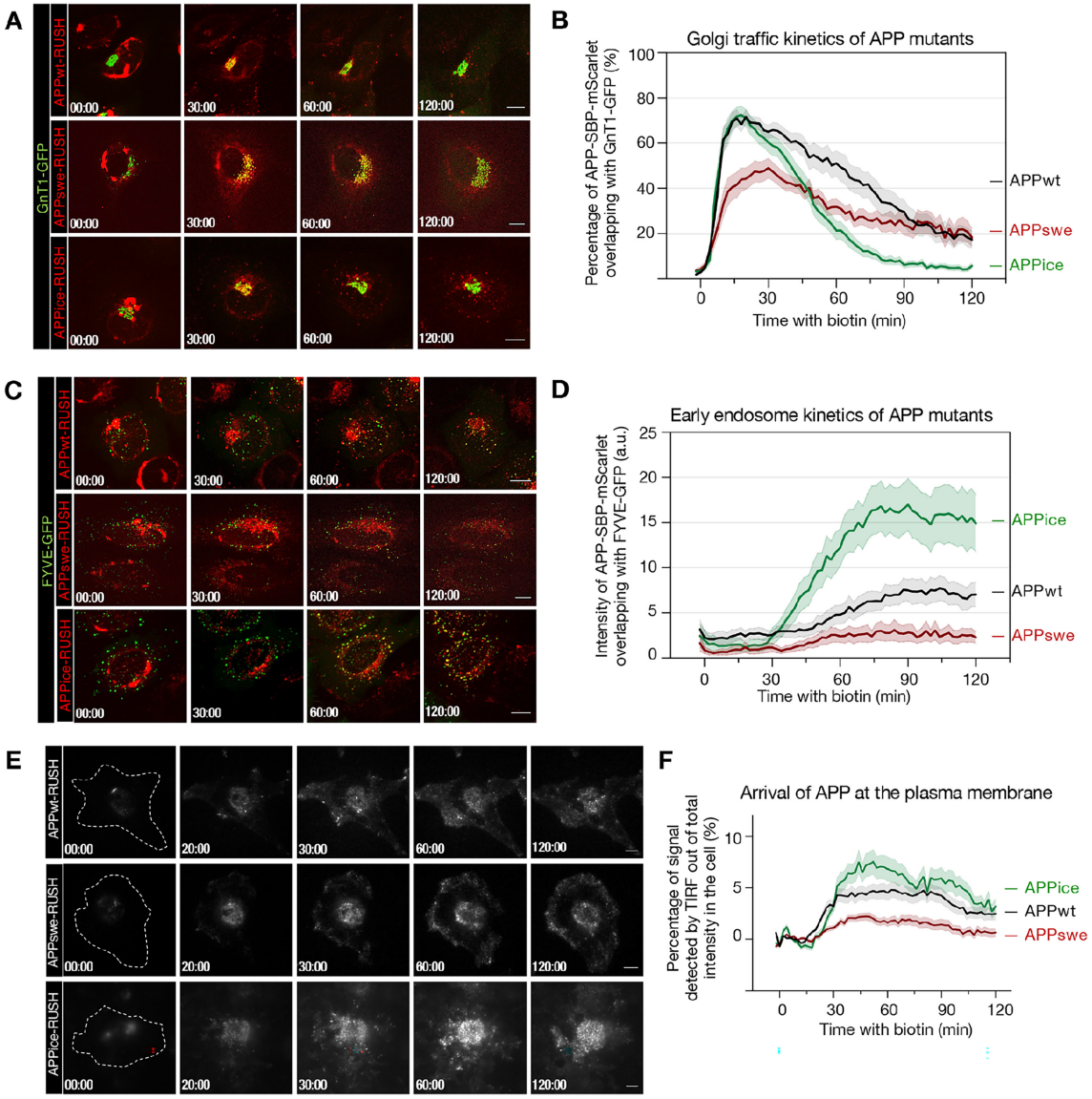

FIGURE 4 | Trafficking of APP is altered by the Swedish and Icelandic mutations. (A) Monolayers of HeLa cells stably expressing WT-, Swedish- or Icelandic-APP RUSH constructs (red) (clone E2, C7 or F10, respectively) were transfected with GnT1-GFP (Golgi marker, green). Biotin was added at time 00:00 (min:s), and real-time dual-colour images of live cells were acquired at indicated time point (min:s) after biotin addition using a spinning disc microscope. Images show maximum projections of z-stacks. Scale bar represents 10 μm. (B) Percentages of APPwt-, APPswe- or APPice-SBP-mScarlet overlapping with GnT1-GFP at indicated time points were calculated using a Mander's coefficient from z-stack image of individual cell similar to the cell represented in (A) using FIJI/ImageJ [39]. Curves represent mean ± SEM, $n \geq 15$ cells from three independent experiments. (C) Live cell imaging experiments were carried out as described in (A) with the early endosome marker, FYVE-GFP (green). (D) Intensity of APPwt-, APPswe- or APPice-SBP-mScarlet (red) overlapping with FYVE-GFP at indicated time points were calculated using a Mander's coefficient from z-stack images of individual cells similar to the cell represented in (C) using FIJI/ImageJ [39]. The curves represent mean value ± SEM, $n \geq 13$ cells from three independent experiments. (E) Monolayers of HeLa cells stably expressing WT-, Swedish- or Icelandic-APP RUSH constructs (red) (clone E2, C7 or F10, respectively) were imaged using a TIRF microscope. Biotin was added at time 00:00 (min:s), and real-time TIRF images of cell surface signal only were acquired at indicated time points (min:s) after biotin addition. Scale bar represents 10 μm. (F) In individual cells from (E), the percentage of signal detected by TIRF of the total mScarlet intensity in the cell, detected by confocal microscopy, was quantified over time. The curves represent mean ± SEM, $n \geq 28$ cells from three independent experiments.

endosomes and with only low levels delivered to the cell surface [22]. To determine the levels of the Swedish and APPice transported to the plasma membrane, total internal reflection fluorescence (TIRF) microscopy was performed during a 2-h biotin time course on live cells (Figure 4E). To optimise the TIRF set-up, HeLa cells transfected with the focal adhesion marker, Paxillin, were added to the sample coverslip to establish the TIRF angle and TIRF focus in order to capture the arrival of proteins within the zone of the plasma membrane (Figure S4). As expected, in the absence of biotin, there was minimal signal detected by TIRF for APPwt, APPswe and APPice RUSH cargoes (Figure 4E,F). The APP RUSH cargoes arrived at the plasma membrane at 30 min onwards after biotin addition (Figure 4E,F). The level of mScarlet signal at the plasma

membrane was quantified based on the total cellular mScarlet fluorescence signal detected in the cell using a standard confocal microscopy angle. Only ~5% of APPwt was detected by TIRF at the plasma membrane at peak levels, indicating limited transport of APPwt-SBP-mScarlet to the plasma membrane (Figure 4E,F). The APP level at the plasma membrane was lower for APPswe (~2.5%) and higher for APPice (7.5%) (Figure 4E,F). These data show that (1) only a minor portion of APP is sorted directly from the Golgi apparatus towards the plasma membrane and (2) the APPswe mutation had the lowest level at the cell surface compared with APPwt and APPice.

2.6 | APPswe Is Extensively Processed by the Amyloidogenic Pathway in the Golgi Apparatus

To characterise the intracellular processing of APP bearing the Swedish or Icelandic mutations and to compare with the APPwt, we initially determined the processing of non-RUSH, fluorescent protein-tagged APP constructs at steady state. HeLa cells were transfected with APPwt, APPswe or APPice tagged with mCherry, treated with DAPT, or not for 16 h before cell lysis. Cell lysates were analysed by immunoblotting with either the APP Y188 or APP-WO2 antibodies (Figure 5A,B). Non-transfected HeLa cells

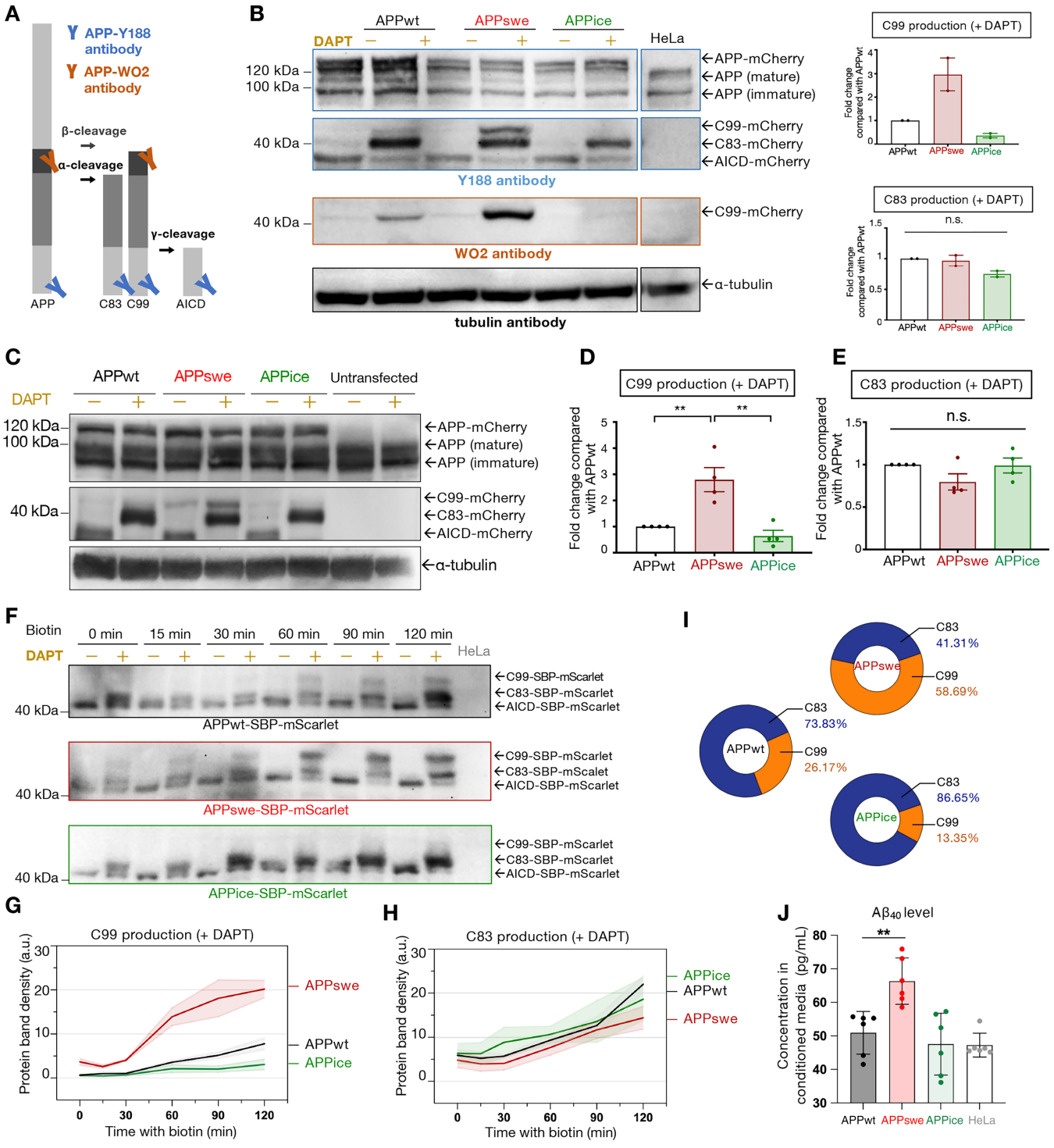

FIGURE 5 | The processing of APP along the secretory pathway is altered by the Swedish and Icelandic mutations. (A) Sequential cleavage of full-length APP by the α, β and γ-secretases leads to the formation of C83, C99 and AICD fragments. APP full length and APP fragments have different molecular weights and are all recognised on their C-terminus by the APP-Y188 antibody, whereas APP-WO2 antibody recognised only APP full length and C99 fragment. (B) Monolayers of HeLa cells were transfected with either APPwt-Cherry, APPswe-Cherry or APPice-Cherry were treated with either 500 nM DAPT or DMSO (carrier control) for 16 h before cell lysis. Untransfected HeLa cells were used as control. Cell lysates were then analysed by immunoblotting using the APP-Y188 antibody (rabbit) or APP-Wo2 (mouse) antibody. Signal in the 40–50 kDa region (size of the cleavage products) is shown. Levels of C99 and C83 (APPY188 blot) were quantified in the presence of DAPT by fold change compared with C99 or C83 produced by APPwt and normalised against total protein level. Bars represent mean ± SEM from two independent experiments. (C) Primary mouse cortical neurons were transfected with APPwt-, APPswe- or APPice-mCherry at DIV3 in the absence or presence of 500 nM DAPT treatment for 16 h. Cell lysates were harvested at DIV4 and analysed by immunoblotting using anti APP antibody (Y188, rabbit). The membrane was then stripped and re-probed with an anti α-tubulin antibody (mouse). (D-E) Levels of C99 and C83 were quantified in the presence of DAPT from (C) by fold change compared with C99 or C83 produced by APPwt, normalised against total protein level. Data represent mean ± SEM from four independent experiments from two mice. $^{**}p < 0.01$ analysed by two-tailed *t*-test with Welch's correction. (F) Monolayers of HeLa cells stably expressing WT-, Swedish- or Icelandic-APP RUSH constructs (clone E2, C7 or F10, respectively) were treated with either 500 nM DAPT or DMSO (carrier control) for 16 h. Biotin was added for 0, 15, 30, 60, 90 or 120 min before cell lysis. Cell lysates were then analysed by immunoblotting using the APP-Y188 antibody (rabbit). Signal in the 40–50 kDa region (size of the cleavage products) is shown. Full immunoblots are shown in Figure S2. (G,H) Protein band density of C99 (G) and C83 (H) were quantified and normalised to the total protein level. Curves represent mean ± SEM from three independent experiments. (I) Ratio of C83 and C99 production 120 min after the addition of biotin (steady state) was quantified for APPwt, APPswe and APPice. (J) Monolayers of HeLa cells stably expressing WT-, Swedish- or Icelandic-APP RUSH constructs (clone E2, C7 or F10, respectively) were treated with biotin overnight (16 h). Conditioned media were harvested and analysed by ELISA for secreted $A\beta_{40}$. WT HeLa cells without APP RUSH protein expression were included as a background Aβ level control. Bars represent mean ± SD from three independent experiments. $^{**}p < 0.01$ analysed by two-tailed *t*-test with Welch's correction.

were included as a negative control. Based on the size of the bands and their abundance following DAPT treatment, the bands detected with Y188 antibody at 41, 39 and 36 kDa represent C99-mCherry, C83-mCherry and AICD-mCherry, respectively (Figure 5A,B). APP-WO2 reactivity with the 41 kDa band confirmed the identity of the C99-mCherry, the β-secretase cleavage product (Figure 5B). In the presence of DAPT, APPswe-mCherry showed a higher level of C99-mCherry, and APPice-mCherry showed a lower level C99-mCherry, compared with APPwt-mCherry (Figure 5B). Quantitation revealed a 2.9-fold higher level of C99-mCherry from APPswe-mCherry, and APPice-mCherry revealed a 2.8-fold lower level of C99-mCherry, compared with APPwt-mCherry. In contrast, the levels of the α-secretase cleavage product, C83-mCherry, was similar for the three APP constructs. The differential susceptibility of APPswe-mCherry and APPice-mCherry to BACE1 cleavage is consistent with the literature [36, 37].

To ensure that the relative difference in APP processing of APPswe-mCherry and APPice-mCherry observed in HeLa cells reflects the secretase processing events in neurons, primary mouse cortical neurons were transfected with APPwt-, APPswe- or APPice-mCherry and treated with DAPT, or not for 16 h and lysates analysed by immunoblotting with the APP-Y188 antibody (Figure 5C). APPswe-mCherry generated a 2.8-fold higher level of C99-mCherry compared with APPwt in the presence of DAPT in primary mouse neurons (Figure 5D), consistent with the observations in HeLa cells (Figure 5B). APPwt, APPswe and APPice-mCherry produced similar levels of C83-mCherry (Figure 5E). Hence, the relative levels of β- and α-secretase processing of APPwt, APPswe and APPice-mCherry in primary neurons and HeLa cells are similar, indicating that the HeLa cell system using stable cell lines should provide biologically relevant information on spatial and temporal events associated with mutant APP processing.

To determine the spatial–temporal relationships of APP processing arising from APPwt, APPswe and APPice, the HeLa RUSH cell lines were used (E2, C7 and F10, respectively) and the C-terminal cleavage products were analysed by immunoblotting using APP-Y188 antibody at different time points after ER release by addition of biotin (Figure 5F, Figure S2). In the absence of the γ-secretase inhibitor DAPT, the levels of C83-SBP-mScarlet and C99-SBP-mScarlet were very low throughout the 2-h biotin time course, as expected for the three APP constructs (Figure 5F), indicating a fast processing of the intermediate cleavage products into AICD. In the presence of DAPT, high levels of C99-SBP-mScarlet were detected from APPswe-SBP-mScarlet during the biotin time course (Figure 5F,G). In contrast, low levels of C99-SBP-mScarlet were detected from APPice-SBP-mScarlet throughout the entire time course (Figure 5F,G). At steady state (120 min after biotin addition), the ratio of the C99/C83 products was different between APPwt, APPswe and APPice (Figure 5F,I). Compared with APPwt, the level of β-secretase BACE1 processing was increased for APPswe and decreased for APPice. Furthermore, a substantial amount of the APPswe was cleaved by BACE1 at 60 min after biotin addition, which correlates with the time APPswe was localised in the Golgi. The level of the α-cleavage product, C83-SBP-mScarlet, was similar across the three APP RUSH proteins during the biotin time course (Figure 5H). These data indicate there is limited direct competition between the α- and β-secretases for APP processing and that the familial mutations SWE and ICE selectively affect the β-secretase cleavage of APP.

To further confirm the processing of APPswe by the secretases in the late Golgi, an experiment was performed at 20°C to block transport out of the TGN [43]. HeLa E2 and C7 cells were incubated with biotin for 15 min at 37°C to release APP from the ER and then incubated at 20°C for 90 min in the presence or in the absence of DAPT (Figure S5A). The lengthy incubation at 20°C was required to accumulate APP in the Golgi and because the secretases are known to be very inefficient catalytically at the lower temperature of 20°C [10]. Immunofluorescence confirmed that both APPwt and APPswe were restricted to the

Golgi, and a minor level in the ER, following biotin addition and the 90-min chase at 20°C (Figure S5B), confirming that the APP cargo had been blocked from exiting the Golgi. In the presence of DAPT, C83-SBP-mScarlet was the major component detected for APPwt, whereas both C83-SBP-mScarlet and C99-SBP-mScarlet were detected for APPswe (Figure S5C), confirming that both α and β-secretase cleavages of APPswe take place in the Golgi. In the absence of DAPT, AICD was detected for both APPwt and APPswe, whereas the levels of C83-SBP-mScarlet and C99-SBP-mScarlet fragments were minimal (Figure S5C), also confirming that γ-secretase processing of both C99-SBP-mScarlet and C83-SBP-mScarlet occurred prior to the Golgi exit.

To examine the secretion of Aβ peptides from cells expressing APPwt, APPswe and APPice, HeLa E2, C7 and F10 stable cell lines were cultured in the presence of biotin for 16 h. The conditioned media was harvested and analysed for secreted Aβ using an enzyme-linked immunosorbent assay (ELISA) specific for $A\beta_{40}$ (Figure 5J). Non-transfected HeLa cells were included as a background control. $A\beta_{40}$ secretion by E2 (APPwt) and F10 (APPice) cells was similar to the $A\beta_{40}$ level secreted by non-transfected HeLa cells (Figure 5J). On the other hand, C7 cells expressing the APPswe secreted significantly more $A\beta_{40}$ than E2 or F10 cells (Figure 5J). The elevated secretion of $A\beta_{40}$ by the C7 line expressing APPswe demonstrates that the BACE1 processing of APPswe-SBP-mScarlet in the Golgi generates Aβ, which can be secreted from the cell by post-Golgi export pathways.

2.7 | Golgi Trafficking of APPswe Is Modified by Secretase Processing

To investigate whether the difference observed in the Golgi trafficking kinetics of the Swedish and APPice mutants is a consequence of secretase-mediated processing in the secretory pathway, we utilised two secretase inhibitors C3 and DAPT to inhibit the β- and γ-secretases, respectively. The effect of C3 and DAPT was initially assessed by immunoblotting of cell extracts at steady state (120 min after biotin addition) (Figure 6A,B). Inhibition of the β- and γ-secretases by the inhibitors was confirmed by immunoblotting. C83-SBP-mScarlet and C99-SBP-mScarlet accumulated with DAPT treatment (inhibition of γ-secretase) alone. Low levels of C99-SBP-mScarlet and AICD-SBP-mScarlet were detected after treatment with both C3 and DAPT (Figure 6A,B). The levels of C83-SBP-mScarlet were unaffected by C3 and DAPT treatment, demonstrating that α-secretase was unaffected by C3 (Figure 6A).

Anterograde trafficking of APPwt and APPswe in live cells was analysed in the presence of C3 and DAPT and the co-localisation of APP with the Golgi marker quantitated (Figure 6C). The Golgi trafficking kinetics of APPwt was similar with or without C3 treatment (Figures 6C and S6A). As there was only a low-level β-secretase processing of APPwt in the Golgi, this finding shows that the drug treatment per se did not affect APP Golgi transport. In contrast, the Golgi trafficking kinetics of APPswe was affected by C3 and DAPT treatment (Figures 6D,E and S6B, Movies S6 and S7). In the absence of C3 and DAPT, the APPswe-SBP-mScarlet signal became dim 60 min after biotin addition, with only a few post-Golgi fluorescent puncta detected (Figure 6D, Movie, S6), consistent with the earlier experiment (Figure 3B). However, in the presence of C3 and DAPT, abundant bright APPswe-SBP-mScarlet puncta were observed following the Golgi exit (Figures 6D and S6B, Movie S7). Quantitative analysis of APPswe-SBP-mScarlet trafficking revealed that APPswe-SBP-mScarlet showed a rapid increase in fluorescence at the Golgi, following 15-min treatment with biotin, with a higher peak of APPswe fluorescence overlapping with GnT1-GFP in the presence of C3 and DAPT compared with the carrier control (Figure 6E). APPswe is subsequently delivered to the endosomal system, with accumulation in the early and late endosomes/lysosomes in the presence of C3 and DAPT (Figure 6F,G). These data show that inhibition of β- and γ-secretase processing protects APPswe from the early β-secretase cleavage in the Golgi, which then displayed a trafficking profile similar to APPwt. Therefore, the altered intracellular trafficking and distribution of APPswe is directly related to β-secretase processing of APPswe in the Golgi apparatus.

3 | Discussion

Numerous studies have shown that Aβ can be generated in both the secretory and endocytic pathways [5]; but, the location(s) that contribute to enhanced Aβ production under pathogenic conditions has not been clearly defined. APPswe is the most studied of the APP familial mutations; however, the impact on the trafficking and processing of APPswe had previously been analysed using indirect approaches, with some studies indicating Aβ production within the secretory pathway [10, 28–30] and other studies within endocytic pathway [30–33]. To directly analyse the relationship between trafficking and processing, we have used the RUSH system to define the kinetics of trafficking of newly synthesised wild-type and mutant APP and the timing of APP cleavage as it is transported along the secretory and endocytic pathways. Consequently, the spatial–temporal events of APP trafficking have been aligned with the spatial–temporal events of secretase processing.

APPwt was transported to the Golgi, with a peak at 20 min, following release from the ER by addition of biotin, and then subsequently transported to the early endosomes. Our data indicate that APPwt-SBP-mScarlet is directly transported from the Golgi apparatus to early endosomes as only low levels of APP reached the cell surface, as detected by TIRF. Previously we have shown that inhibition of endocytosis of untagged APP does reduce the efficiency of Golgi to early endosome transport of APP [22], confirming that the delivery to early endosomes does not require APP endocytosis from the cell surface. The majority of APPwt-SBP-mScarlet processing occurred during its exit from the Golgi and on arrival in early endosomes.

A key finding of this study is that the major site of APPswe processing differs from the APPwt. The Swedish double mutation is located adjacent to the BACE1 cleavage site and is known to be more efficiently cleaved by BACE1 than APPwt [35, 36]. APPswe displayed a longer Golgi 'residency time' compared with APPwt. The intensity of APPswe fluorescent signal, but not the APPwt and APPice signals, waned during its transit through the Golgi and low levels of APPswe cargo were observed to exit the Golgi. The loss of APPswe signal is likely due to a high level of secretase processing and degradation, during its Golgi trafficking,

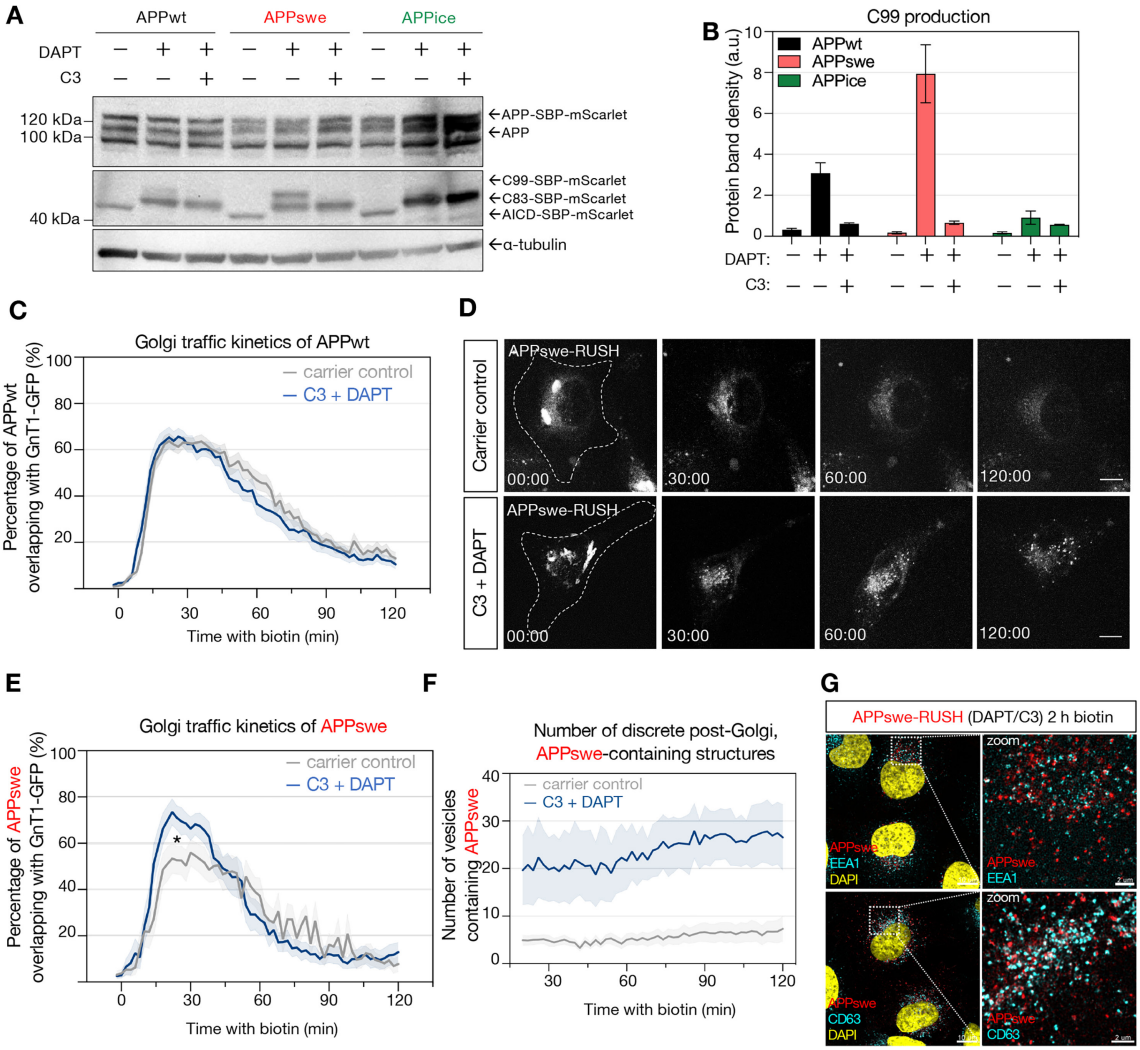

FIGURE 6 | Trafficking kinetics of Swedish APP is altered by the inhibition of secretase processing. (A) Monolayers of HeLa cells stably expressing WT-, Swedish- or Icelandic-APP RUSH constructs (clone E2, C7 or F10, respectively) were treated with either DMSO (carrier control), 5 μM DAPT or with the combination of 2 μM C3 and 5 μM DAPT for 16 h. Biotin was added for 120 min before cell lysis. Cell lysates were analysed by immunoblotting using an anti-APP antibody (Y188, rabbit). Signal around the size of the cleavage products (40–50 kDa) is shown. (B) Protein band density of C99 was quantified and normalised to the total protein level. Bars represent mean ± SEM from three independent experiments. (C) Monolayers of HeLa E2 cells stably expressing Str-Ii and APPwt-SBP-mScarlet was transfected with GnT1-GFP (green) (see images Figure S4A). Cells were treated with either DMSO (carrier control) or the combination of 2 μM C3 and 5 μM DAPT for 16 h. In individual cells, percentages of APPwt-SBP-mScarlet overlapping with GnT1-GFP were calculated by Mander's coefficient from z-stacks using FIJI/ImageJ batch analysis macro [39]. The curves represent mean value ± SEM, $n \geq 20$ cells from three independent experiments. (D) Monolayers of HeLa C7 cells stably expressing Str-Ii and APPswe-SBP-mScarlet was treated with either DMSO (carrier control) or the combination of 2 μM C3 and 5 μM DAPT for 16 h. Biotin was added at time 00:00 min:s, and live cell imaging was carried out at indicated time points (min:s) after biotin addition using a spinning disc microscope. Images show maximum projections of z-stacks. Scale bar represents 10 μm. (E) In individual cells, percentages of APPswe-SBP-mScarlet overlapping with GnT1-GFP in the presence or absence of C3 and DAPT were calculated by Mander's coefficient from z-stacks using FIJI/ImageJ [39]. Dual-colour images are represented in Figure S4B). The curves represent mean value ± SEM, $n \geq 14$ cells from three independent experiments. *$p < 0.05$ (at peak time $t = 26$ min) analysed by two-tailed t-test with Welch's correction. (F) The number of discrete post-Golgi, APPswe-containing structures were quantified in individual cells from (D) using FIJI/ImageJ. The curves represent mean value ± SEM, $n \geq 14$ cells from three independent experiments. (G) Monolayers of HeLa C7 cells stably expressing Str-Ii and APPswe-SBP-mScarlet were treated with 2 μM C3 and 5 μM DAPT for 16 h and fixed 2 h after biotin addition. Cells were permeabilised, blocked and stained with anti-EEA1 antibody (early endosome) or CD63 antibody (late endosome/lysosome). Scale bar represents 10 μm.

resulting in the loss of the membrane-bound mCherry/mScarlet fluorescence. Elevated levels of the BACE1 cleavage product, C99-SBP-mScarlet, was detected in cells expressing APPswe compared with APPwt, particularly in the early time points (0–60 min after addition of biotin) when the majority of APPswe resided in the Golgi. Strikingly, the loss of post-Golgi APPswe-SBP-mScarlet was rescued by the inhibition of β- and γ-secretases, demonstrating that β-secretase cleavage of APPswe takes place in the Golgi, which in turn limits the availability of the delivery of full-length APPswe to post-Golgi compartments. A previous study using in vitro assays also demonstrated that the APPswe could be processed in the Golgi/TGN [10]; however,

the contribution of the Golgi to the total Aβ levels was not quantified in that study. Our findings show that the late Golgi/TGN is the predominant intracellular site for the enhanced processing of APPswe by BACE1 and γ-secretase.

The Aβ generated from the secretase processing of APPswe was secreted, suggesting that Aβ is likely to be exported via Golgi export pathways. We have previously demonstrated that Aβ can be secreted from the TGN of neurons [21]. The export of Aβ from the Golgi is likely to be very efficient, given the dedicated constitutive transport pathway for soluble and membrane proteins, whereas the pathways for secretion of Aβ generated within the endosomal system are likely to be indirect and inefficient [9], such as secretion via exosomes from the late endosomes [32].

Only a low level of APPwt was processed prior to Golgi exit. Our previous studies have shown that APP and BACE1 are segregated immediately on exiting the ER and traverse the Golgi stacks with only a low level of co-localisation detected [20]. Our findings that APPswe is extensively processed in the late Golgi indicates either that the partitioning of APP and BACE1 is insufficient to control the processing of a mutant APP with a higher affinity for BACE1 than APPwt, or that the membrane partitioning of APP and BACE1 is affected by the Swedish mutations, which are proximal to the transmembrane domain. Either of these two mechanisms would indicate that the co-localisation of APPwt and BACE1 within the Golgi cisternae is very finely controlled and any perturbation of Golgi membranes, which enhances the co-localisation of APPwt and BACE1 and/or affinity of substrate/enzyme, could result in a significant increase in intracellular Aβ production.

The HeLa cell system in this study allowed stable cell lines with very similar levels of the expression of RUSH constructs to be compared for quantitative analysis. Previous studies have demonstrated shared characteristics of APP and BACE1 trafficking between primary neurons and cultured HeLa cells [20–22]. These include the selective AP1- and AP4-mediated sorting pathways for BACE1 and APP from the TGN, respectively [21, 22], and the partitioning of BACE1 and APP in the early Golgi [20], indicating the physiological relevance of the HeLa cell model [21]. As the α- and β-secretase processing of APPwt, APPswe and APPice fluorescent proteins was demonstrated to be very similar at steady state for primary mouse neurons and APP HeLa cell lines, the RUSH analysis using the stable HeLa cells is likely to reflect the pathways in primary neurons. The use of RUSH to quantify the temporal events of APP trafficking and processing in non-dividing primary neurons is problematic due to the variable expression level within the cell population, arising from transient expression systems using lentiviral delivery.

In contrast to APPswe, the protective APPice mutation was transported more rapidly through the Golgi apparatus to the endosomal compartments compared with APPwt. From 30 to 60 min after ER release, the bulk of APPice had trafficked through the Golgi en route to early endosomes, whereas a large portion of APPwt still remained in the Golgi at the same time period. Not surprisingly, very little β-secretase processing product was detected with APPice throughout the entire time course. The basis for the more rapid Golgi transport of APPice is not clear, but may be associated with efficient partitioning into membrane domains and/or limited processing events in the Golgi.

The majority of wild-type APP-SBP-mScarlet is processed by the α-secretase pathway, consistent with the processing of endogenous APP [44]. A similar level of the α-secretase product C83 was detected in the APPwt and mutant APP HeLa cell lines. This finding supports the independent regulation of APP processing by the amyloidogenic and non-amyloidogenic pathways, rather than a direct competition between the α- and β-secretase enzymes [5]. The TGN has recently been demonstrated to be a site for α-secretase processing in HeLa cells and primary neurons [45], which could account for the non-amyloidogenic processing of APPswe.

Based on the findings in this article, the location of APP BACE1 processing and the production of Aβ are summarised in Figure 7. The majority of BACE1 processing of APPwt occurs in the early endosomes, whereas the majority of BACE1 processing of APPswe occurs in the late Golgi/TGN. A previous study has also proposed different sites for the processing of APPwt and APPswe based on a selective block in processing

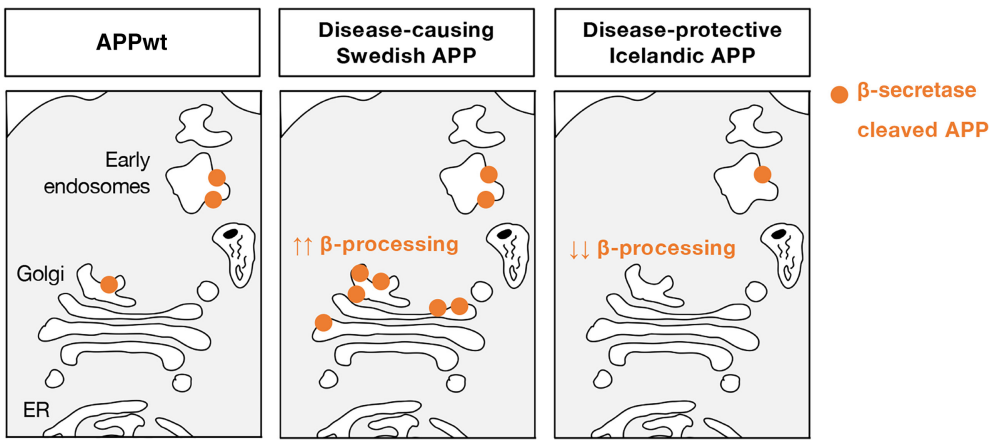

FIGURE 7 | Intracellular sites of amyloidogenic processing of APPwt and disease-related mutations. Wild-type and familial disease-related APP mutants differ in their preferential sites for secretase processing. The disease-causing APPswe is associated with an enhanced β-secretase processing in the Golgi apparatus compared with APPwt. The majority of β-secretase processing of APPwt occurs in early endosomes while the disease-protective APPice has only low levels of β-secretase processing in either the Golgi or early endosomes.

APPwt, but not APPswe, by the inhibitor of the vacuolar H+-ATPase, bafilomyin A1 [46], and our data here support and extend to this conclusion by direct analysis of the processing sites. Only low levels of APPice were processed by BACE1 in the Golgi or endosomes, consistent with the reduced affinity of the APPice for BACE1 [37]. Aβ is generated very rapidly following BACE1 cleavage of APP by γ-secretase processing. The outcome of the differential processing by BACE1 is that the half-life of APPswe is considerably shorter than that of either APPwt or APPice.

The consequence of an alteration in the intracellular trafficking of APPswe and steady-state distribution of full length APP may result in additional effects beyond increasing the production of Aβ, such as (1) the processed APP products arising from APPswe within the secretory pathway may not reach their destinations to perform physiological functions; (2) dysregulated production of Aβ in the secretory network could lead to organellar abnormalities, including but not limited to Golgi fragmentation [47] and ER stress [48]; (3) reduced levels of APPswe in endosomal system and plasma membrane, compared with APPwt, may impact on the ability of APP to function normally in maintenance of a neuronal network [49]; and, as discussed above, (4) an important implication of β-secretase processing of APP in the early-secretory pathway is that Aβ production in the Golgi provides a potential pathway for efficient secretion of Aβ.

The identification of the Golgi as a preferential site for APPswe processing raises a number of questions in relation to the development of Alzheimer's disease. What effect does the production of Aβ in the Golgi have on disease initiation? Observations over 25 years have reported that the neuronal Golgi structure is 'fragmented' in Alzheimer's disease and directly contributes to the pathology of the disease [50, 51]. Aβ is also known to mediate fragmentation of the Golgi ribbon in cell-based systems [47, 50]. Given that the APPswe mutation is responsible for the genesis of EOAD, it is critical to determine the consequence of APPswe processing and Aβ production in the Golgi on the Golgi morphology, post-Golgi trafficking pathways, cellular organisation and intracellular toxicity leading to neuronal cell death [52].

In conclusion, our data confirm that the Golgi is the major site for the proteolytic processing of newly synthesised APPswe mutation and production of Aβ. In addition, the findings have revealed different intracellular locations for the preferential cleavage and Aβ production of APPswe and APPwt. The findings highlight the importance of understanding the mechanisms regulating APP processing in the early-secretory pathway, which may provide novel therapeutic options to reduce the generation of Aβ under pathogenic conditions.

4 | Materials and Methods

4.1 | Culture of Mammalian Cell Lines

Mycoplasma-free authentic HeLa cells were maintained in Dulbecco's modified Eagle medium (DMEM) (Gibco, Thermo Fisher Scientific) supplemented with 10% v/v foetal bovine serum (FBS), 2 mM L-glutamine and 100 units/μL penicillin and 0.1% w/v streptomycin (C-DMEM). HEK293T packaging cells were maintained in C-DMEM without penicillin and streptomycin (C-DEMEM-P/S). All cell lines were cultured as adherent monolayers, passaged with TrypLE (Thermo Fisher Scientific) according to manufacturer's instructions, and incubated at 37°C in a humidified incubator with 10% CO_2. Cells were routinely tested for mycoplasma contamination using the MycoAlert Mycoplasma Detection Kit (Lonza, Switzerland).

4.2 | Generation of Mutant APP RUSH Constructs by Site-Directed Mutagenesis

The APP_{695} isoform was used in all constructs, as this is the major isoform in human neurons. Str-Ii_APPwt-SBP-mCherry, pCDH_Str-Ii and pCDH_APPwt-SBP-mCherry were kind gifts from Dr Franck Perez and Dr Gaelle Boncompain (Institut Curie, Paris, France). APPwt-mCherry was generated by Wei Hong Toh [53]. mCherry tag was swapped for mScarlet tag using the RUSH restriction sites SbfI and FseI. Site-directed mutagenesis (SDM) was performed to generate the Swedish mutation using primers 5′ ATCTCTGAAGTGAATCTGGATGCAGAATTC 3′ (forward) and 5′ GAATTCTGCATCCAGAT-TCACTTCAGAGAT 3′ (reverse). The Icelandic mutation was generated using primers 5′ GTGAA-GATGGATACAGAATTCCGACAT 3′ (forward) and 5′ ATGTCGGAATTCTGTATCCATCTTC-AC 3′ (reverse). SDM was performed by polymerase chain reaction (PCR). After 2 min of initial denaturation at 98°C, 20 cycles of PCR were carried out, each with 15 s of denaturation at 98°C, 30 s of annealing at 68°C and 5 min of extension at 72°C. After 15 min of final extension at 72°C, the PCR products were collected, pooled together and purified using the QIAquick PCR purification kit (Qiagen, Germany) with an elution volume of 30 μL. Purified DNA (30 μL) was digested by 10 μL of DpnI restriction enzyme overnight at 37°C to remove parental plasmids. Digested PCR products (10 μL) were transformed into competent *Escherichia coli* DH5α bacterial cells (Bioline, Australia) for plasmid production. Single bacterial colonies were picked and inoculated into 3 mL LB with 50 μg/mL ampicillin or kanamycin and cultured overnight at 37°C under agitation. Plasmid preparations were performed using a Promega mini-prep kit (Promega, USA) following manufacturer's instructions. Purified plasmids were then sequenced by AGRF (Australian Genome Research Facility, Australia) using Sangers sequencing. DNA plasmids were produced using a NucleoBond Xtra-Midi kit (Machery-Nagel, Germany) according to manufacturer's instructions.

4.3 | Generation of HeLa Cell Lines Stably Expressing APP RUSH System

APP RUSH recombinant lentiviruses were generated by calcium phosphate transfection of low-passage HEK293T packaging cells with lentiviral plasmids following the ratio of 1pCMV-VSV-G, 2psPAX2 and 2pCDH_Str-Ii (hook virus only) or pCDH_APP-SBP-mScarlet (cargo virus only) plasmids as previously described [45]. Low-passage HeLa cells (P6) were transduced with APP RUSH lentiviruses and incubated at 37°C, 10% CO_2 for 24 h before the virus-containing media were replaced with fresh C-DMEM and cells incubated for 48 h before they

were detached with TrypLE and re-suspended in 2 mM EDTA. Cells positive for mScarlet fluorescence were sorted through a BD Influx cell sorter (BD Bioscience), using flow cytometry facility at Murdoch Children's Research Institute (MCRI), as single cells into 96-well plates as well as a polyclonal population into 10-cm dishes. Monoclonal cell colonies were expanded to confluence in 96-well plates and passaged sequentially in 24- and 6-well plates. Clones with more than 80% of cells expressing the RUSH proteins with a good ER retention were selected and further expanded.

4.4 | Culture and Transfection of Primary Mouse Cortical Neurons

All experiments carried out on animals were in accordance with animal ethics guidelines approved by the Animal Ethics Committee, The University of Melbourne (Approval ID: 1914968.1). Primary mouse cortical neurons were prepared from the collected embryos of a pregnant mouse (C57BL/6) at gestational days 15 and 16 and cultured as previously described [45]. Primary cortical neurons were plated at a density of 0.6×10^5 cells/well (24-well plates) and 5×10^5 cells/well (6-well plates), and cultured in neurobasal medium supplemented with 2.5% B-21, 0.25% GlutaMAX and 100 units/μL penicillin and 0.1% streptomycin (complete NBM) (Life Technologies, USA). Lipofectamine2000 transfection reagent (Thermo Fisher Scientific) was used to transfect neurons following manufacturer's instructions. Briefly, 1-μg plasmid DNA was mixed with 2 μL of Lipofectamine reagent, and the cells were incubated with the transfection mixture for 2–4 h. Cells were incubated with half conditioned media and half fresh media after transfection mixtures were removed. Then, 0.5 or 2 μg of plasmid DNA was added per well in 24- or 6-well plates, respectively.

4.5 | Drug Treatment

HeLa cells stably expressing APP RUSH constructs were treated with either DMSO (carrier control) or 500 nM of γ-secretase inhibitor *N*-[*N*-(3,5-difluoreophenacetyl)-1-alanyl]-S-phenylglycine-t-butyl ester (DAPT) (Sigma-Aldrich, Merck, USA) for single-treatment experiments. Cells were incubated with DAPT for 16–20 h in a 37°C incubator with 10% CO_2 before being harvested for western blot analysis or live cell imaging described in the following: In double inhibition experiments, HeLa cells stably expressing APP RUSH constructs were treated with 5 μM of DAPT in combination with 2 μM of the β-secretase/BACE1 inhibitor C3 (Calbiochem, Merck, USA) for 16–20 h before harvesting or imaging. In half-life assays, HeLa cells stably expressing APP RUSH constructs were treated with 50 μg/mL cycloheximide (CHX) (Sigma-Aldrich, Merck, USA) for up to 4 h before cell fixation or lysis. Treatments were performed in a 37°C incubator with 10% CO_2.

4.6 | Trafficking Assays Using the RUSH System

HeLa cells, cultured as monolayers, were either transfected using calcium phosphate [54] or were stably expressing the RUSH system. Transfected cells were incubated for 24 h at 37°C with 10% CO_2. The expressed cargo was retained in the ER in the absence of biotin. D-biotin (Sigma-Aldrich, Merck) was added to the cell monolayer to a final concentration of 40 μM to induce the synchronous release of APP RUSH. Cells were then either fixed at different time points after biotin addition or imaged live. To retain APP RUSH cargo in the Golgi, a 20°C block was carried out; cargo was released from the ER by addition of biotin at 37°C for 15 min, followed by a 5-min incubation on ice, and then incubation at 20°C for 90 min.

4.7 | Live Cell Imaging and TIRF

An inverted Nikon Ti spinning disc microscope (with optical autofocus system and a motorised piezo stage), an Andor Izxon Ultra EM-CCD camera and the MetaMorph imaging system (Molecular Devices, USA) were used for live cell imaging with a 100× oil-immersed objective. For HeLa cells, adherent cell monolayers on 24-mm coverslips were clipped in a metal chamber, maintained in Leibovitz's medium without phenol-red (Thermo Fisher Scientific) and incubated at 37°C for the duration of imaging. For neurons, cells were maintained in C-NBM and incubated at 37°C with 5% CO_2 for the duration of imaging. Images with z-stacks (11 steps, step size 0.4 μm) were captured every 2 min for 120 min after addition of 40 μM D-biotin to the cell monolayer. Laser power and acquisition settings were chosen to avoid photo-bleaching and settings were identical for all imaging. TIRF analysis of live cells was carried out using the same system. Images were collected every 2 s. 'Marker' HeLa cells transfected separately with fluorescently tagged Paxillin, a focal adhesion protein, were added onto the sample coverslip to set up the TIRF angle and focus as an indicator.

4.8 | Indirect Immunofluorescence Analysis

Adherent cell monolayer cultured on coverslips were washed in PBS and fixed in either (1) 4% paraformaldehyde (PFA) (Wako Pure Chemical Industries, Japan) for 10–15 min at room temperature (RT) and quenched with 50 mM NH_4Cl for 10 min or (2) 10% trichloroacetic acid (TCA) on ice for 15 min and quenched with 30 mM glycine for 10 min. Cells were permeabilised with 0.1% Triton X-100 for 4 min and blocked in 5% FBS for at least 15 min. HeLa cells were stained with primary antibodies (diluted in 5% FBS/PBS) either at RT for 1 h or at 4°C overnight. Mouse antibodies to human KDEL (#ab12223, 1/200) and rabbit antibodies to human golgin-97 (#ab84340, 1/400) were purchased from Abcam. Mouse antibodies to human GM130 (#610823, 1/400), EEA1 (#610456, 1/400) and Rab11 (#610656, 1/200) were purchased from BD Biosciences. Mouse antibodies to human CD63 (#sc5275, 1/100) were purchased from Santa Cruz. Rabbit antibodies to human GCC88 have been described [55]. Human antibodies to golgin-245 (p230) have been described [56]. Cells stained with primary antibodies were washed three times in PBS before incubation with conjugated secondary antibodies (diluted 1/400 in 5% FBS/PBS) for 45–60 min at RT. Secondary antibodies used goat anti-mouse immunoglobulin G (IgG): Alexa Fluor 488, goat anti-rabbit IgG–Alexa Fluor 488, goat anti-mouse IgG–Alexa Fluor 568, goat anti-rabbit IgG–Alexa Fluor 568, goat anti-mouse IgG–Alexa Fluor 647, goat anti-rabbit IgG–Alexa Fluor 647 and goat anti-human Alexa Fluor

647 were purchased from Life Technologies. Cells incubated with secondary antibodies were washed three times in PBS and mounted in Mowiol (10% w/v Hopval 5-88, 25% w/v glycerol, 0.1 M Tris in Milli-Q water) containing 1 μg/mL DAPI (#D9542, Sigma-Aldrich).

Super-resolution images (Figure 3E) were acquired with a laser confocal scanning microscope Zeiss LSM880 with Airyscan (Carl Ziess, North Ryde, Sydney) equipped with a 63×1.4 NA Plan-Apochromat (420782-9900-799) oil immersion objective and 32 hexagonal array Airyscan detectors. Images were collected sequentially for multi-colour imaging using super-resolution (SR) Airyscan mode. Images were acquired as z-stacks comprising 8–11 sections with a z-step of 0.159 μm per section, meeting the Nyquist–Shannon sampling rate for axial dimension. Image acquisitions were performed using the Zeiss Zen software (v2.3 SP1).

4.9 | Protein Immunoblotting Analysis

Monolayers of HeLa cells stably expressing the APP RUSH constructs were treated with either DMSO (carrier control) or 500 nM of DAPT (γ-secretase inhibitor) (Sigma-Aldrich) for 16 h. Cell lysates were prepared by extraction with 50 μL per well (12-well plate) of radioimmunoprecipitation assay (RIPA) lysis buffer (50 nM Tris–HCl, pH 7.3, 150 nM NaCl, 0.1 mM EDTA, 1% w/v sodium deoxycholate, 1% v/v Triton X-100, 0.2% w/v NaF, and 100 μM Na_3VO_4) supplemented with 1× cOmplete Mini Protease Inhibitor Mixture (Roche Applied Science, Sigma-Aldrich, Merck) on ice for 30 min. Cell lysates were collected, vortexed for 15 s and centrifuged at 15 000 rpm, 4°C for 15 min. The supernatants were collected and stored at −20°C. The samples were mixed with 1× NuPAGE LDS sample buffer and 1× NuPAGE sample-reducing buffer (Invitrogen, Thermo Fisher Scientific). Samples were denatured at 90–100°C for 10 min and loaded onto a NuPAGE 10% Bis-Tris gel (Thermo Fisher Scientific). Proteins were separated by gel electrophoresis at 150 V for 1.5 h and transferred to a PVDF membrane at 25 V for 2 h. The membrane was blocked in 10% w/v milk–PBS–Tween for 1 h under agitation. The primary antibodies were diluted in PBS–Tween, added onto the membrane and incubated overnight at 4°C. Rabbit antibody to APP (APP-Y188, #ab32136, 1/6000) was purchased from Abcam. Mouse antibody to APP (APP-WO-2, #MABN10, 1/2000) was purchased from Merck Millipore. Mouse antibody to α-tubulin (#T9026, 1/2000) was purchased from Sigma. After the incubation with primary antibodies, the membrane was washed in 0.1% v/v PBS–Tween three times (5 min each) before incubation with HRP-conjugated secondary antibodies for 30 min. Horseradish peroxidase-conjugated goat anti-rabbit IgG (#65-6120) and goat anti-mouse IgG (#62-6520) were purchased from Invitrogen (Thermo Fisher Scientific Australia). After the incubation with secondary antibodies, the membrane was washed three times before being immersed with ECL detecting solution (GE Healthcare) for 2 min. Antibody-bound protein bands were visualised using a ChemiDoc Imaging System (Bio-Rad). Total protein loaded in the lanes was visualised using the lysine-based No-Stain protein-labelling reagent (Thermo Fisher Scientific) according to manufacturer's instructions.

4.10 | Enzyme-Linked Immunosorbent Assay (ELISA)

HeLa cells stably expressing the APP RUSH system were seeded with 1.0×10^5 cells in 12-well plates, and confluent wells were cultured in 300 μL C-DMEM when treated with 40 μM D-biotin for 16 h. Conditioned media were harvested, and a commercial ELISA kit specifically designed to detect Aβ40 (KHB3481, Life Technologies, Thermo Fisher Scientific) was used, following the manufacturer's instructions, to assess the level of secreted Aβ.

4.11 | Quantification of Data and Statistical Analysis

Co-localisation analysis between APP RUSH cargoes and organelle markers from live cell imaging experiments were carried out using a set of FIJI/ImageJ batch analysis macro as previously described [39]. Total intensity and size of particles were calculated using the same FIJI/ImageJ analysis macro approach with raw intensity and particle size as output parameters [39]. Data were plotted as mean ± standard error of mean (SEM) using Prism9 software (GraphPad). Data were analysed by unpaired, two-tailed *t*-tests with Welch's correction using Prism9, where $p<0.05$, 0.01, 0.001 and 0.0001 (*, **, *** and ****, respectively) were considered statistically significant.

For western blot quantification, band intensities across lanes were normalised to the average of three of the major protein bands visualised by the No-Stain total protein labelling reagent. Absolute densities or fold change of C83/C99 levels were plotted as bar graphs (mean ± SEM) and analysed by unpaired, two-tailed *t*-tests with Welch's correction, where $p<0.05$, 0.01, 0.001 and 0.0001 (*, **, *** and ****, respectively) were considered statistically significant.

SR images were processed using Huygens software (Array detector deconvolution module, using a conservative mode and theoretical PSF). Co-localisation analysis was performed using Imaris software (v9.5.1, Oxford Instruments) by applying surface–surface co-localisation XT.

Author Contributions

Conceptualisation: J.W., P.A.G. and L.F. Methodology: J.W. and L.F. Investigation: J.W. and L.F. Resources: P.A.G. and L.F. Writing—original draft: J.W., P.A.G. and L.F. Writing, reviewing and editing: J.W., P.A.G. and L.F. Visualisation: J.W. and L.F. Supervision: P.A.G. and L.F. Funding acquisition: P.A.G. and L.F.

Acknowledgements

Microscopy and image processing were performed at the Biological Optical Microscopy Platform (BOMP), and the Biosciences Microscopy Unit, at the University of Melbourne. This work was supported by funding from the National Health and Medical Research Council of Australia (APP1163862: 2013344). J.W. is supported by a University of Melbourne International Postgraduate Award. We acknowledge Ellie Cho for her expertise in cell quantification, Fiona Houghton for excellent laboratory support and Dr Wei Hong Toh for the APP-mCherry construct. Open access publishing facilitated by The University of Melbourne, as part of the Wiley - The University of Melbourne agreement via the Council of Australian University Librarians.

Conflicts of Interest

The authors declare no conflicts of interest.

Peer Review

The peer review history for this article is available at https://www.webofscience.com/api/gateway/wos/peer-review/10.1111/tra.12932.

References

1. Alzheimer's Association, "2023 Alzheimer's Disease Facts and Figures," *Alzheimer's & Dementia* 19, no. 4 (2023): 1598–1695.

2. Y. T. Wu, A. S. Beiser, M. M. B. Breteler, et al., "The Changing Prevalence and Incidence of Dementia Over Time – Current Evidence," *Nature Reviews. Neurology* 13, no. 6 (2017): 327–339.

3. D. J. Selkoe and J. Hardy, "The Amyloid Hypothesis of Alzheimer's Disease at 25 Years," *EMBO Molecular Medicine* 8, no. 6 (2016): 595–608.

4. S. A. Small and S. Gandy, "Sorting Through the Cell Biology of Alzheimer's Disease: Intracellular Pathways to Pathogenesis," *Neuron* 52, no. 1 (2006): 15–31.

5. J. Z. A. Tan and P. A. Gleeson, "The Role of Membrane Trafficking in the Processing of Amyloid Precursor Protein and Production of Amyloid Peptides in Alzheimer's Disease," *Biochimica et Biophysica Acta - Biomembranes* 1861, no. 4 (2019): 697–712.

6. L. Blaikie, G. Kay, and P. Kong Thoo Lin, "Current and Emerging Therapeutic Targets of Alzheimer's Disease for the Design of Multi-Target Directed Ligands," *Medchemcomm* 10, no. 12 (2019): 2052–2072.

7. C. A. Lane, J. Hardy, and J. M. Schott, "Alzheimer's Disease," *European Journal of Neurology* 25, no. 1 (2017): 1–12.

8. J. P. Greenfield, J. Tsai, G. K. Gouras, et al., "Endoplasmic Reticulum and Trans-Golgi Network Generate Distinct Populations of Alzheimer Beta-Amyloid Peptides," *Proceedings of the National Academy of Sciences of the United States of America* 96, no. 2 (1999): 742–747.

9. W. H. Toh and P. A. Gleeson, "Dysregulation of Intracellular Trafficking and Endosomal Sorting in Alzheimer's Disease: Controversies and Unanswered Questions," *The Biochemical Journal* 473, no. 14 (2016): 1977–1993.

10. H. Xu, D. Sweeney, R. Wang, et al., "Generation of Alzheimer Beta-Amyloid Protein in the Trans-Golgi Network in the Apparent Absence of Vesicle Formation," *Proceedings of the National Academy of Sciences of the United States of America* 94, no. 8 (1997): 3748–3752.

11. B. D. Bennett, S. Babu-Khan, R. Loeloff, et al., "Expression Analysis of BACE2 in Brain and Peripheral Tissues," *The Journal of Biological Chemistry* 275, no. 27 (2000): 20647–20651.

12. I. Hussain, D. Powell, D. R. Howlett, et al., "Identification of a Novel Aspartic Protease (Asp 2) as Beta-Secretase," *Molecular and Cellular Neurosciences* 14, no. 6 (1999): 419–427.

13. S. Sinha, J. P. Anderson, R. Barbour, et al., "Purification and Cloning of Amyloid Precursor Protein Beta-Secretase From Human Brain," *Nature* 402, no. 6761 (1999): 537–540.

14. H. M. Lanoiselee, G. Nicolas, D. Wallon, et al., "APP, PSEN1, and PSEN2 Mutations in Early-Onset Alzheimer Disease: A Genetic Screening Study of Familial and Sporadic Cases," *PLoS Medicine* 14, no. 3 (2017): e1002270.

15. Y. Zhang, H. Chen, R. Li, K. Sterling, and W. Song, "Amyloid Beta-Based Therapy for Alzheimer's Disease: Challenges, Successes and Future," *Signal Transduction and Targeted Therapy* 8, no. 1 (2023): 248.

16. P. V. Burgos, G. A. Mardones, A. L. Rojas, et al., "Sorting of the Alzheimer's Disease Amyloid Precursor Protein Mediated by the AP-4 Complex," *Developmental Cell* 18, no. 3 (2010): 425–436.

17. P. Z. Chia, W. H. Toh, R. Sharples, I. Gasnereau, A. F. Hill, and P. A. Gleeson, "Intracellular Itinerary of Internalised Beta-Secretase, BACE1, and Its Potential Impact on Beta-Amyloid Peptide Biogenesis," *Traffic* 14, no. 9 (2013): 997–1013.

18. Y. C. Januario, J. Eden, L. S. de Oliveira, et al., "Clathrin Adaptor AP-1-Mediated Golgi Export of Amyloid Precursor Protein Is Crucial for the Production of Neurotoxic Amyloid Fragments," *The Journal of Biological Chemistry* 298, no. 8 (2022): 102172.

19. W. H. Toh, P. Z. Cheryl Chia, M. Iqbal Hossain, and P. A. Gleeson, "GGA1 Regulates Signal-Dependent Sorting of BACE1 to Recycling Endosomes, Which Moderates Aβ Production," *Molecular Biology of the Cell* 29, no. 2 (2018): 191–208.

20. L. Fourriere, E. H. Cho, and P. A. Gleeson, "Segregation of the Membrane Cargoes, BACE1 and Amyloid Precursor Protein (APP) Throughout the Golgi Apparatus," *Traffic* 23 (2022): 158–173.

21. J. Z. A. Tan, L. Fourriere, J. Wang, F. Perez, G. Boncompain, and P. A. Gleeson, "Distinct Anterograde Trafficking Pathways of BACE1 and Amyloid Precursor Protein From the TGN and the Regulation of Amyloid-Beta Production," *Molecular Biology of the Cell* 31, no. 1 (2020): 27–44.

22. W. H. Toh, J. Z. Tan, K. L. Zulkefli, F. J. Houghton, and P. A. Gleeson, "Amyloid Precursor Protein Traffics From the Golgi Directly to Early Endosomes in an Arl5b- and AP4-Dependent Pathway," *Traffic* 18, no. 3 (2017): 159–175.

23. Y. Prabhu, P. V. Burgos, C. Schindler, G. G. Farias, J. G. Magadan, and J. S. Bonifacino, "Adaptor Protein 2-Mediated Endocytosis of the Beta-Secretase BACE1 Is Dispensable for Amyloid Precursor Protein Processing," *Molecular Biology of the Cell* 23, no. 12 (2012): 2339–2351.

24. C. Perdigao, M. A. Barata, M. N. Araujo, F. S. Mirfakhar, J. Castanheira, and A. C. Guimas, "Intracellular Trafficking Mechanisms of Synaptic Dysfunction in Alzheimer's Disease," *Frontiers in Cellular Neuroscience* 14 (2020): 72.

25. A. Peric and W. Annaert, "Early Etiology of Alzheimer's Disease: Tipping the Balance Toward Autophagy or Endosomal Dysfunction?" *Acta Neuropathologica* 129, no. 3 (2015): 363–381.

26. X. Wang, T. Huang, G. Bu, and H. Xu, "Dysregulation of Protein Trafficking in Neurodegeneration," *Molecular Neurodegeneration* 9 (2014): 31.

27. L. Fourriere and P. A. Gleeson, "Amyloid Beta Production Along the Neuronal Secretory Pathway: Dangerous Liaisons in the Golgi?" *Traffic* 22, no. 9 (2021): 319–327.

28. G. Thinakaran, D. B. Teplow, R. Siman, B. Greenberg, and S. S. Sisodia, "Metabolism of the "Swedish" Amyloid Precursor Protein Variant in Neuro2a (N2a) Cells. Evidence That Cleavage at the "Beta-Secretase" Site Occurs in the Golgi Apparatus," *The Journal of Biological Chemistry* 271, no. 16 (1996): 9390–9397.

29. C. Haass, C. A. Lemere, A. Capell, et al., "The Swedish Mutation Causes Early-Onset Alzheimer's Disease by Beta-Secretase Cleavage Within the Secretory Pathway," *Nature Medicine* 1, no. 12 (1995): 1291–1296.

30. R. G. Perez, S. L. Squazzo, and E. H. Koo, "Enhanced Release of Amyloid Beta-Protein From Codon 670/671 "Swedish" Mutant Beta-Amyloid Precursor Protein Occurs in Both Secretory and Endocytic Pathways," *The Journal of Biological Chemistry* 271, no. 15 (1996): 9100–9107.

31. A. Kinoshita, H. Fukumoto, T. Shah, C. M. Whelan, M. C. Irizarry, and B. T. Hyman, "Demonstration by FRET of BACE Interaction With the Amyloid Precursor Protein at the Cell Surface and in Early Endosomes," *Journal of Cell Science* 116, no. Pt 16 (2003): 3339–3346.

32. L. Rajendran, M. Honsho, T. R. Zahn, et al., "Alzheimer's Disease Beta-Amyloid Peptides Are Released in Association With Exosomes,"

Proceedings of the National Academy of Sciences of the United States of America 103, no. 30 (2006): 11172–11177.

33. S. Schilling, A. Pradhan, A. Heesch, et al., "Differential Effects of Familial Alzheimer's Disease-Causing Mutations on Amyloid Precursor Protein (APP) Trafficking, Proteolytic Conversion, and Synaptogenic Activity," *Acta Neuropathologica Communications* 11, no. 1 (2023): 87.

34. G. Boncompain, S. Divoux, N. Gareil, et al., "Synchronization of Secretory Protein Traffic in Populations of Cells," *Nature Methods* 9, no. 5 (2012): 493–498.

35. X. D. Cai, T. E. Golde, and S. G. Younkin, "Release of Excess Amyloid Beta Protein From a Mutant Amyloid Beta Protein Precursor," *Science* 259, no. 5094 (1993): 514–516.

36. M. Citron, T. Oltersdorf, C. Haass, et al., "Mutation of the Beta-Amyloid Precursor Protein in Familial Alzheimer's Disease Increases Beta-Protein Production," *Nature* 360, no. 6405 (1992): 672–674.

37. T. Jonsson, J. K. Atwal, S. Steinberg, et al., "A Mutation in APP Protects Against Alzheimer's Disease and Age-Related Cognitive Decline," *Nature* 488, no. 7409 (2012): 96–99.

38. M. P. Schutze, P. A. Peterson, and M. R. Jackson, "An N-Terminal Double-Arginine Motif Maintains Type II Membrane Proteins in the Endoplasmic Reticulum," *The EMBO Journal* 13, no. 7 (1994): 1696–1705.

39. J. Wang, E. H. Cho, P. A. Gleeson, and L. Fourriere, "Quantification of Golgi Entry and Exit Kinetics of Protein Cargoes," *Methods in Molecular Biology* 2557 (2023): 559–572.

40. S. S. Hebert, L. Serneels, A. Tolia, et al., "Regulated Intramembrane Proteolysis of Amyloid Precursor Protein and Regulation of Expression of Putative Target Genes," *EMBO Reports* 7, no. 7 (2006): 739–745.

41. S. Mosser, J. R. Alattia, M. Dimitrov, et al., "The Adipocyte Differentiation Protein APMAP Is an Endogenous Suppressor of Aβ Production in the Brain," *Human Molecular Genetics* 24, no. 2 (2015): 371–382.

42. T. Wegierski, K. Gazda, and J. Kuznicki, "Microscopic Analysis of Orai-Mediated Store-Operated Calcium Entry in Cells With Experimentally Altered Levels of Amyloid Precursor Protein," *Biochemical and Biophysical Research Communications* 478, no. 3 (2016): 1087–1092.

43. M. S. Ladinsky, C. C. Wu, S. McIntosh, J. R. McIntosh, and K. E. Howell, "Structure of the Golgi and Distribution of Reporter Molecules at 20°C Reveals the Complexity of the Exit Compartments," *Molecular Biology of the Cell* 13, no. 8 (2002): 2810–2825.

44. P. H. Kuhn, H. Wang, B. Dislich, et al., "ADAM10 Is the Physiologically Relevant, Constitutive Alpha-Secretase of the Amyloid Precursor Protein in Primary Neurons," *The EMBO Journal* 29, no. 17 (2010): 3020–3032.

45. J. Z. A. Tan and P. A. Gleeson, "The Trans-Golgi Network Is a Major Site for Alpha-Secretase Processing of Amyloid Precursor Protein in Primary Neurons," *The Journal of Biological Chemistry* 294, no. 5 (2019): 1618–1631.

46. C. Haass, A. Capell, M. Citron, D. B. Teplow, and D. J. Selkoe, "The Vacuolar H(+)-ATPase Inhibitor Bafilomycin A1 Differentially Affects Proteolytic Processing of Mutant and Wild-Type Beta-Amyloid Precursor Protein," *The Journal of Biological Chemistry* 270, no. 11 (1995): 6186–6192.

47. G. Joshi, Y. Chi, Z. Huang, and Y. Wang, "Aβ-Induced Golgi Fragmentation in Alzheimer's Disease Enhances Aβ Production," *Proceedings of the National Academy of Sciences of the United States of America* 111, no. 13 (2014): E1230–E1239.

48. J. X. Pan, D. Sun, D. Lee, et al., "Osteoblastic Swedish Mutant APP Expedites Brain Deficits by Inducing Endoplasmic Reticulum Stress-Driven Senescence," *Communications Biology* 4, no. 1 (2021): 1326.

49. S. Ludewig and M. Korte, "Novel Insights Into the Physiological Function of the APP (Gene) Family and Its Proteolytic Fragments in Synaptic Plasticity," *Frontiers in Molecular Neuroscience* 9 (2016): 161.

50. H. Haukedal, G. I. Corsi, V. P. Gadekar, et al., "Golgi Fragmentation—One of the Earliest Organelle Phenotypes in Alzheimer's Disease Neurons," *Frontiers in Neuroscience* 17 (2023): 1120086.

51. J. A. Martinez-Menarguez, M. Tomas, N. Martinez-Martinez, and E. Martinez-Alonso, "Golgi Fragmentation in Neurodegenerative Diseases: Is There a Common Cause?" *Cells* 8, no. 7 (2019): 748.

52. D. M. Walsh and D. J. Selkoe, "Amyloid Beta-Protein and Beyond: The Path Forward in Alzheimer's Disease," *Current Opinion in Neurobiology* 61 (2020): 116–124.

53. W. Toh, "The Intracellular Trafficking Pathways of β-Secretase and the Amyloid Precursor Protein in Alzheimer's Disease" (PhD thesis, Biochemistry and Molecular Biology, University of Melbourne, 2015).

54. M. Jordan, A. Schallhorn, and F. M. Wurm, "Transfecting Mammalian Cells: Optimization of Critical Parameters Affecting Calcium-Phosphate Precipitate Formation," *Nucleic Acids Research* 24, no. 4 (1996): 596–601.

55. M. R. Luke, L. Kjer-Nielsen, D. L. Brown, J. L. Stow, and P. A. Gleeson, "GRIP Domain-Mediated Targeting of Two New Coiled-Coil Proteins, GCC88 and GCC185, to Subcompartments of the Trans-Golgi Network," *The Journal of Biological Chemistry* 278, no. 6 (2003): 4216–4226.

56. J. Kooy, B. H. Toh, J. M. Pettitt, R. Erlich, and P. A. Gleeson, "Human Autoantibodies as Reagents to Conserved Golgi Components. Characterization of a Peripheral, 230-kDa Compartment-Specific Golgi Protein," *The Journal of Biological Chemistry* 267 (1992): 20255–20263.

Supporting Information

Additional supporting information can be found online in the Supporting Information section.